Applied Mathematical Modelling 41 (2017) 1–24

Contents lists available at ScienceDirect

Applied Mathematical Modelling

journal homepage: www.elsevier.com/locate/apm

Mathematical modeling of resonant linear vibratory conveyor with electromagnetic excitation: simulations and experimental results

Željko V. Despotović[a,*], Djordje Urukalo[a], Milan R. Lečić[b], Aleksandar Ćosić[a]

[a] University of Belgrade, Mihajlo Pupin Institute, 15 Volgina, 11060 Belgrade, Serbia
[b] University of Belgrade, Faculty of Mechanical Engineering, 16 Kraljice Marije, 11000 Belgrade, Serbia

ARTICLE INFO

Article history:
Received 7 May 2016
Revised 29 August 2016
Accepted 14 September 2016
Available online 22 September 2016

Keywords:
Vibratory conveyor
Modeling
Lagrange equation
Electromagnetic excitation
Thyristor converter
Simulations

ABSTRACT

Vibratory conveyors are commonly used in industry for transporting a wide variety of bulk and particulate materials. Various control structures based on state observers can be found in the literature. However, they are mostly based on simplified mathematical models. In order to obtain a more precise state observer, and consequently better performance and (or) control quality, more detailed mathematical model of the resonant vibratory conveyor is required. Mathematical model of a resonant linear vibratory conveyor driven by an electromagnetic excitation force is presented. Derivation of the mathematical model is based on the kinetic and potential energies, dissipative function of the mechanical system, and Lagrangian formulation. A simulation model is implemented on the basis of the derived mathematical equations. The simulation results are presented and compared to the experimental results obtained by a real industrial vibratory conveyor.

1. Introduction

Vibratory conveying represents one of the most efficient ways of moving bulk and particulate materials. This method is used in many material processing technologies (drying, dust collection, classification, dosing, compaction, crushing, dehydration, etc.). The most commonly used machines are vibratory conveyors, feeders, vibratory elevators and bunker dispensers [1,2].

Vibratory conveyors are used to transport a variety of different bulk materials and solids over short to medium distances. They are also suitable for conveying a wide range of material types. In general, granular materials are handled far simpler than pulverized, and flat or irregular shapes better than spherical [2]. Vibratory feeders containing a linear vibratory conveyor are widely used in industry in a wide range of applications (from processing pharmaceuticals to discharging coal from silos). The flow-promoting property of vibratory motion, combined with the ability of removing and even distribution of material from a bin or hopper opening, make vibratory feeders and vibratory conveyors very popular. Vibratory conveyors are often used in extreme conditions (in a vacuum and/or at elevated temperatures) [3]. A very specific application of mechanical vibration and vibratory conveyors with electromagnetic excitation can be encountered in the systems for capturing and transportation of regolith particles on the surface of the Moon and Mars [4].

* Corresponding author. Fax: +381 116776583.
E-mail addresses: zeljko.despotovic@pupin.rs, zdespot@hotmail.com (Ž.V. Despotović), djordje.urukalo@pupin.rs (D. Urukalo), mlecic@mas.bg.ac.rs (M.R. Lečić), aleksandar.cosic@pupin.rs (A. Ćosić).

http://dx.doi.org/10.1016/j.apm.2016.09.010
0307-904X/

Symbols

$\vec{F}$	Electromagnetic excitation force.
k	Stiffness of the leaf springs.
k_x, k_y	Stiffness coefficients of the bumpers in horizontal and vertical direction, respectively.
$\underline{q}$	Vector of generalized coordinates.
u	Displacement of the base in the horizontal direction relative to the equilibrium position.
w	Displacement of the base in the vertical direction, relative to the equilibrium position.
p	Displacement of the vibratory trough relative to the base.
E_k, E_p	Kinetic and potential energies, respectively.
Q_j	Generalized non-conservative forces.
p_{st}, f_{st}	Static spring deformations of elastic holders and rubber bumpers, respectively.
E	Modulus of elasticity.
I	Moment of inertia of the console cross section.
f_x, f_y	Horizontal and vertical springs deformations, respectively.
m_B	Mass of the base.
v_B	Velocity of the COM of the base.
m_K	Mass of the vibratory trough together with an elastic holder.
J_B, J_C	Moments of inertia of the base and the trough.
$\vec{v}_{C,rel}$	Relative velocity of point C.
Q_{wj}	Damping-generalized forces.
$\underline{Q}_{\Omega}$	Vector of generalized excitation force.
A	Area enclosed by the total magnetic flux.
H_z, H_b	Magnetic fields in the air gap and bronze, respectively.
N	Number of inductor windings.
R_c	Total electrical resistance of EVA coil.
i	Actual current of EVA coil.
Ni	Total Ampere-turns.
B	Magnetic field induction.
W_m^*	Magnetic co-energy.
$\Im_1^e$	Lagrangian of the electromechanical subsystem.
$\Re_1^e$	Rayleigh dissipative function.
d	Thickness of the bronze pole.
D	Distance between the inductor and movable armature at equilibrium position.
z	Air gap in an actuator magnetic circuit.
$L(z)$	Inductance of the electromagnetic actuator.
$e(\dot{z}, z, t)$	Counter-electromotive force (CEMF).
$\tilde{A}, \tilde{B}, \tilde{C}$	System state, input and output matrices, respectively.
$\tilde{x}, \tilde{u}, \tilde{y}$	System states, inputs and outputs, respectively.
F	External mechanical force.
m_{k0}, m_k	Mass of the empty and filled trough, respectively.
f	Mains frequency.
f_r	Linear resonant frequency.
Φ	Dissipative function of the system.
Φ_S	Magnetic flux in the air gap and bronze.
Φ_A	Magnetic flux through surface A of the pole end.
μ_0, μ_{Fe}	Permeability of the air and iron.

Greek letters

α^*	Phase angle.
τ	Electrical time constant of the EVA coil.
τ_p	Time constant of the displacement p.
ω	Angular mains frequency.
ω_{res}	Resonant angular frequency of the conveyor.
λ_t	Empirical dimensionless correction coefficient.
β_x	Damping coefficients of the horizontal and vertical components of the shock absorbers, respectively.
β_y	Damping coefficient of the vertical shock absorbers.
λ	Total magnetic flux.
φ	Angle of rotation of the base relative to the equilibrium position.

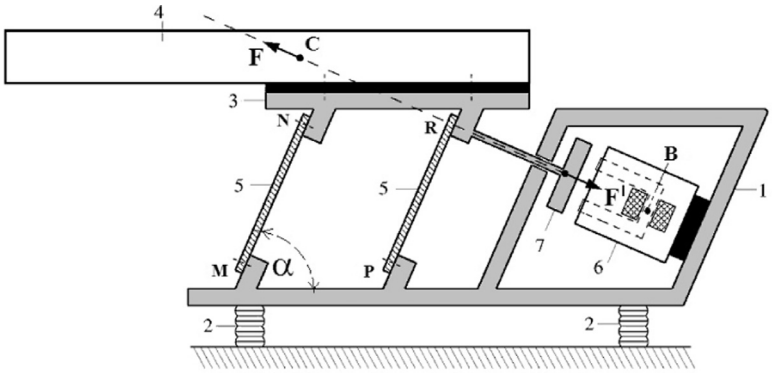

Fig. 1. Typical construction of electromagnetic vibratory conveyor with EVA.

From a microscopic point of view, the process of vibratory conveying is very complicated and needs to be treated by the laws of statistical physics. The theoretical investigations and studies of processing and conveying of granular materials are given in a comprehensive list of references [1,5–7].

From a macroscopic point of view, vibratory conveying process is based on repetition of micro-throw of particles. Vibrations of a plate or trough on which a loose material is placed, are transferred to the particles of the material, so it exhibits the characteristics of a viscous fluid, thus, it is easier to achieve its extraction, conveying and dosing. The size and shape of particle micro-throws depend on the frequency of oscillation of the conveying plate, where the material is placed. Productivity or capacity of a vibratory conveyor, i.e. the mass (gravimetric) flow of material, for a given vibratory frequency, directly depends on the average value of micro-particle throws and the vibratory width (double amplitude of oscillations) of the conveying plate. The mass flow varies over a very wide range, depending on the particular industrial application: 50 g/h-fine powder dosing in the pharmaceutical industry, 100t/h-cement industry, up to 1000t/h-coke and crude iron production. Optimal conveying for the majority of bulk materials is carried out in the frequency range 10–150 Hz and amplitude range 0.1–10 mm, depending on the type of applied drive [1,2,8–10].

In most cases, these conveying systems operate in the resonance mode, and consequently, the excitation and maintenance of the system in the state of oscillations require relatively low energy consumption [11–14].

Vibratory-conveying drives with electromagnetic vibratory actuator (EVA) are very popular in the process industry of bulk materials. These drives provide a simple and easy control of bulk material mass-flow. Compared to inertial and mechanical unbalanced drives, electromagnetic drives are simple mechanical constructions (without any rotating parts, gearboxes or belt transmission), quite robust, compact, and reliable in operation. In addition, these drives are characterized by very high efficiency and simple maintenance. It is possible to provide precise control of the bulk material mass flow by adjusting the amplitude of oscillations of the vibratory conveyor [9,10].

In order to further improve and optimize the process of bulk material conveying by the vibratory conveyor drives, it is important to search and track the resonant frequency and provide precise control of the oscillation amplitude. This problem is comprehensively treated in the literature [11–14].

The mathematical models used in the associated control structures are based on appropriate simplifications. Firstly, the impact between vibratory conveyor base and its elastic supports is neglected. One of the essential elements of the control system is the state observer [14–16]. However, in order to obtain a high quality estimate at the output of the state observer, and therefore accomplish an appropriately high performance and (or) control quality, it is necessary to have a detailed mathematical model of the resonant vibratory conveyor with electromagnetic excitation, which takes into account the neglected effects mentioned above.

The previously mentioned reasons are the main motivation for deriving a more detailed mathematical model of the resonant vibratory conveyor presented in this paper. Derivation of the mathematical model is based on calculation of the kinetic and potential energies, dissipative function of the mechanical system, and Lagrangian formulation, as well. Also, a set of simulation results is presented and compared to the experimental results obtained by a real industrial vibratory conveyor.

2. Description of the typical construction of an electromagnetically excited linear vibratory conveyor

Typical arrangement of an electromagnetic vibratory conveyor includes the driving part, which basically comprises one EVA, as shown in Fig. 1. The most important functional parts, having a crucial influence on the dynamic behavior of the linear vibratory conveyor, are situated within this construction.

The *base* (1) of vibratory conveyor rests on the machine foundation via *damping shock absorbers* i.e. *buffers* (2). These elastic elements transfer the load from the conveyor to the machine foundation during oscillation of the *load carrying element* (LCE) (3) which is fixed to a *vibratory trough* (4) in which the material being conveyed is placed. The LCE is attached to the base by elastic *holders-leaf springs* (5). These holders are actually comprised of the "sandwich" of flexible thin elastic

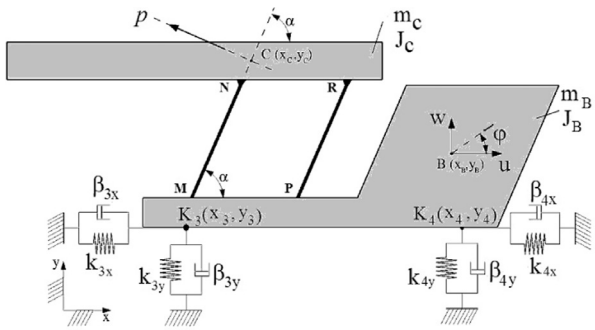

Fig. 2. Mechanical model of vibratory conveyor without EVA.

plates (leafs) based on composite materials very resistant to dynamic and static stress. The holders are inclined at an angle α with respect to the base, so that their direction is normal to the direction of the excitation force generated by the EVA. The basic elements of the EVA are inductor (6) and armature (7). From electrical point of view, EVA is predominantly an inductive load. The electromagnetic excitation force, $\vec{F}$, is generated by electrical current through EVA coil. If the EVA coil is supplied by an impulse current, force $\vec{F}$ will also be pulsating [8–11]. This force provides accumulation of potential energy by the elastic holders.

The accumulated potential energy is released in the form of a return stroke of the elastic holders and vibratory through, denoted by reactive force $\vec{F}'$. Due to this effect, the movement and bouncing of particulate materials are accomplished, leading to conveying of material loaded on the vibratory trough. A very important detail in this construction is that the directions of the forces $\vec{F}$ and $\vec{F}'$, must be along a line passing the center of mass (COM) of the base and the COM of the vibratory trough with LCE (point C). In this way, a directed motion of the vibratory trough and the consequent movement of the conveyed material particles are achieved [17].

Elastic holders (5) are in fact the leaf springs made of n-leafs, where each leaf is of length $\overline{MN} = \overline{PR} = l$, width b, and thickness h. Although the leaf springs can be made of steel, more recently they are being made of special composite materials. These materials belong to the group of so-called *Kelvin materials* characterized by a high elasticity, as described in [18–20]. This means that two forces are present in the holders (5): the elastic force linearly proportional to deformations and damping force linearly proportional to the first derivative of deformations. The corresponding coefficients of proportionality are k and β. Therefore, by their physical nature the holders (5) are in fact damping-elastic elements.

The damping shock absorbers (2) are in fact rubber elastic bumpers. They are used to damp vibrations transmitted from the conveyor structure to foundation of the machine and present damping-elastic elements, as well [21]. On the other hand, they are made of rubber and these dampers are modeled as damping-elastic elements with two degrees of freedom, detailed in references [18,21–24]. In this paper, the bumpers are modeled as two-dimensional structures, as presented in Fig. 2. The equivalent stiffness coefficients of the bumpers are k_x and k_y, while the equivalent viscosity coefficients of the dampers are β_x and β_y.

The mechanical model of a vibratory conveyor without EVA is depicted in Fig. 2. The vibratory conveyor is modeled as a mechanical system consisting of rigid bodies with appropriate internal and external connections. Therefore, the system consists of two rigid bodies, the transporter's base and vibratory trough with the holders, i.e. composite leaf-springs. It is assumed that the masses, geometry, and the corresponding moments of inertia are known. These two rigid bodies are connected by composite springs *MN* and *PR* of known characteristics (k and β). The base is linked to the foundation of the machine at points K_3 and K_4 by horizontal and vertical damping-elastic elements of known characteristics (k_x, k_y and β_x, β_y).

It is assumed that motion of the vibratory system is planar and that it is realized in the plane of a stationary coordinate system Oxy. It is easily observed that the system has four degrees of freedom, so the vector of generalized coordinates has the form $\underline{q} = (q_1, q_2, q_3, q_4)^T = (p, u, w, \varphi)$, [9,10]. Herein, u and w are displacements of the base in the horizontal and vertical directions, respectively, relative to the equilibrium position of the system. Angle φ is the angle of rotation of the base relative to the equilibrium position of the system. Linear coordinate p is displacement of the vibratory trough together with the elastic holder, relative to the base.

3. The differential equations of motion of the vibratory conveyor

Motion of a mechanical system of a finite number of degrees of freedom in the configuration space of generalized coordinates q_j is described by Lagrange equation of the second kind:

$$\frac{d}{dt}\left(\frac{\partial E_k}{\partial \dot{q}_j}\right) - \frac{\partial E_k}{\partial q_j} = -\frac{\partial E_p}{\partial q_j} + Q_j \ \ (j = 1, 2, \ldots s), \tag{1}$$

where the following notation is used: E_k – kinetic energy, E_p – potential energy, and Q_j – generalized non-conservative forces. Kinetic energy is a function of generalized coordinates q_j and all generalized velocities $\dot{q}_j$ for a system of stationary connections.

In general, the differential equations of motion of a mechanical system derived by using Lagrange equation of the second kind are nonlinear. However, the observed mechanical system oscillates during operation with a small amplitude about its stable equilibrium, i.e. it performs low oscillations. In this case, the nonlinear differential equations of motion can be linearized.

Linearization of differential equations defined by Eq. (1) requires that the kinetic and potential energies, as well as the so-called dissipative function, are quadratic forms of the corresponding variables q_j and $\dot{q}_j$. Therefore, instead of direct linearization of nonlinear equations Eq. (1), the process of linearization can be conducted through expansion of the kinetic and potential energies in appropriate series around the stable equilibrium and taking finite number of terms: up to the second order for the kinetic and potential energies, and up to the first order for the non-conservative forces.

3.1. Potential energy of the system

For the considered mechanical system, three terms of the potential energy can be noticed, i.e. $E_p = E_{p1} + E_{p2} + E_{p3}$. The first term is potential energy due to elastic forces of the leaf springs, the second term is potential energy due to gravity for the base and vibratory trough together with the LCE, while the third term represents potential energy due to elastic forces of the elastic bumpers ((2) in Fig. 1). This means that potential energy of the system takes the following form [25–27]:

$$E_p = \frac{1}{2}k_1(p + p_{1,st})^2 + \frac{1}{2}k_2(p + p_{2,st})^2 + m_B g(y_B - y_{B,0}) + m_K g(y_C - y_{C,0}) + \frac{1}{2}k_{3x}(f_{3x} + f_{3x,st})^2 + \frac{1}{2}k_{3y}\left(f_{3y} + f_{3y,st}\right)^2 + \frac{1}{2}k_{4x}\left(f_{4x} + f_{fx,st}\right)^2 + \frac{1}{2}k_{4y}\left(f_{4y} + f_{4y,st}\right)^2. \quad (2)$$

Here, $y_{B,0}$ and $y_{C,0}$ are the coordinates of points B and C in the equilibrium, while p_{st} and f_{st} are the static spring deformations of elastic holder and rubber bumper, respectively. All static deformations are determined from the equilibrium conditions of the system.

Approximately, the expression for potential energy of the system having s degrees of freedom, has the following form [26,27]:

$$E_p = \frac{1}{2}\sum_{i=1}^{s}\sum_{j=1}^{s} k_{ij}q_i q_j. \quad (3)$$

Stiffness coefficients represent the corresponding partial derivatives of the potential energy at the state of equilibrium:

$$k_{ij} = \left(\frac{\partial E_p}{\partial q_i \partial q_j}\right)_0. \quad (4)$$

3.1.1. Potential energy of the forces in the elastic holders that connect the base and LCE

The elastic holders ((5) in Fig. 1) are in fact leaf springs from the group of flexion springs. These leaf springs, such as elastic cantilever beams of equal length, are equally loaded by flexion moment of force $\vec{F}$. The displacements of end points P and R are perpendicular to the console and approximately equal to the relative coordinate p for small oscillations about the equilibrium point. Movement of p is also deformation of the cantilever beam as a result of the acting force. It can be easily obtained that the stiffness coefficient of the leaf spring is $k = 3EI/l^3$, where E is the modulus of elasticity and I is the moment of inertia of the console cross section. The total deformation of each of these two consoles at an arbitrary point is $p + p_{st}$, so the potential energy accumulated in them at an arbitrary position is:

$$E_p = \frac{1}{2}k_1(p + p_{1,st})^2 + \frac{1}{2}k_2(p + p_{2,st})^2. \quad (5)$$

Static deformation can be found from the relative equilibrium conditions of the vibratory trough having elastic holders relative to the base. Two other terms, E_{p2} and E_{p3}, in the expression for potential energy E_p are determined in a similar fashion. The system is firstly brought into an arbitrary position relative to the equilibrium, and then the expression is reduced to a quadratic form.

3.1.2. Potential energy due to gravity of the base, vibratory trough together with LCE, and elastic forces of rubber bumpers.

Oscillations of the considered mechanical system are monitored in a stationary coordinate system Oxy. Let us assume that the mechanical system is located at an arbitrary position with respect to its own equilibrium position at an arbitrary time instant. The potential energy due to gravity is determined by observing arbitrary positions of the centers of gravity B and C, as shown in Fig. 3.

Without any loss of generality, let us assume that the first step is transforming the considered system by using the generalized coordinate u along Ox direction, and that the second step is transforming the observed system by using the generalized coordinate w along Oy direction. The third step is rotation of the whole system by an angle φ, and finally, the

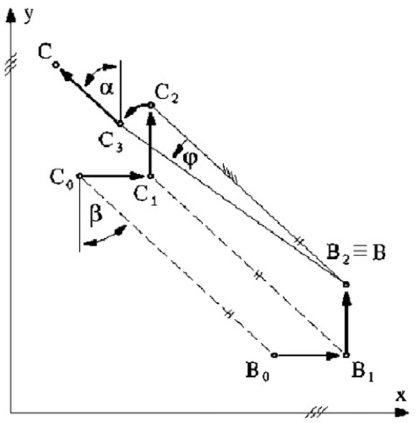

Fig. 3. Schematic representation of the base's center of gravity movement from equilibrium position B_0 to an arbitrary position B, and the vibratory trough's center of gravity movement from equilibrium position C_0 to an arbitrary position C.

fourth step is expressing the relative displacements of the elastic holders and the trough together with LCE with respect to the base by the generalized coordinate p. Positions of the characteristic points of the system are shown in Fig. 3.

In order to determine the potential energy due to gravity, bearing in mind that the zero level is arbitrary, it is assumed for simplicity that system is in the equilibrium. In this way, the potential energy due to gravitational force is:

$$E_{p2} = m_B g(y_B - y_{B,0}) + m_K g(y_C - y_{C,0}), \tag{6}$$

where $y_{B,0}$ and $y_{C,0}$ are coordinates of points B and C at equilibrium. Fig. 3 shows that $y_B - y_{B,0} = w$, i.e. potential energy due to gravity of the base is equal to $m_B g w$. For potential energy of the trough and elastic holders, it is necessary to determine vector $\vec{C_0C}$. From Fig. 3 it can be seen that vector $\vec{C_0C} = \vec{C_0C_1} + \vec{C_1C_2} + \vec{C_2B} + \vec{BC_3} + \vec{C_3C}$. It is easy to notice, that the projection of vector $\vec{C_0C}$ on axis Oy is:

$$\left(\overline{C_0C}\right)_y = y_C - y_{C,0} = w - \overline{C_2B}cos\alpha + \overline{C_2B}cos(\alpha + \varphi) + pcos\alpha. \tag{7}$$

By applying the appropriate formula for addition of cosines, we arrive at expression suitable for the required approximation:

$$\left(\overline{C_0C}\right)_y = w + \overline{C_2B}cos\alpha\,(cos\varphi - 1) - \overline{C_2B}sin\alpha sin\varphi + pcos\alpha. \tag{8}$$

Finally, an expression for the potential energy of gravity of the base and vibratory trough with the bracket is obtained:

$$E_{p2} = m_B g w + m_K g\left(w + \overline{C_2B}cos\alpha\,(cos\varphi - 1) - \overline{C_2B}sin\alpha sin\varphi + pcos\alpha\right). \tag{9}$$

For determination of potential energy forces in elastic bumpers E_{p3}, it is sufficient to observe arbitrary position of one of the two damping shock absorbers ((2) in Fig. 1).

The elastic absorbers are modeled as spring-damping elements in the horizontal and vertical directions, as shown in Fig. 1. The vertical spring-damping element is attached to the surface at the point D while the horizontal one is fixed at point E. Both are connected to the base at point K. Length $\overline{KB}$ and angle γ are constants defined by the geometry of the considered mechanical system. Deformation of the spring element is equal to the difference of the spring length between an arbitrary position and the one at the state of equilibrium. The deformation of the vertical spring is $f_y = \overline{DK} - \overline{DK_0}$, while the horizontal spring deformation is $f_x = \overline{EK} - \overline{EK_0}$.

In Fig. 4 it is shown that vector $\vec{DK}$ can be expressed as the sum of the corresponding vectors:

$$\vec{DK} = \vec{DK_0} + \vec{K_0K}. \tag{10}$$

The same can be obtained for vector $\vec{EK}$:

$$\vec{EK} = \vec{EK_0} + \vec{K_0K}. \tag{11}$$

On the other hand, with reference to Fig. 4, vector $\vec{K_0K}$ is:

$$\vec{K_0K} = \vec{K_0K_1} + \vec{K_1K_2} + \vec{K_2B} + \vec{BK}. \tag{12}$$

The horizontal and vertical projections of vector $\vec{K_0K}$ are equal to the sum of projections of the corresponding vectors. By using addition formulae, we obtain expressions for the horizontal and vertical projections of vector $\vec{K_0K}$:

$$\begin{aligned}\left(\overline{K_0K}\right)_x &= u + \overline{KB}cos\gamma - \overline{KB}cos\gamma cos\varphi + \overline{KB}sin\gamma sin\varphi,\\ \left(\overline{K_0K}\right)_y &= w + \overline{KB}sin\gamma - \overline{KB}sin\gamma cos\varphi - \overline{KB}cos\gamma sin\varphi.\end{aligned} \tag{13}$$

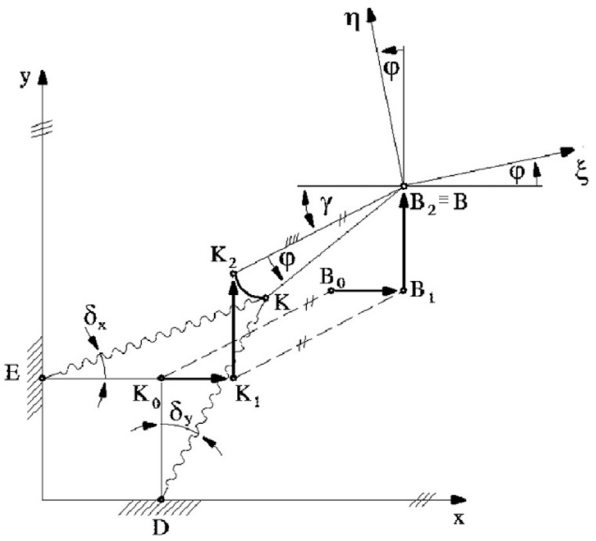

Fig. 4. Schematic diagram of moving end point K of springs EK and DK from equilibrium point K_0 to an arbitrary point K.

Since lengths of the springs are much greater than their deformations, i.e. angles δ_y and δ_x are very small (Fig. 4), then we can say that $\overline{DK} \approx (\overline{DK})_y = \overline{DK_0} + (\overline{K_0K})_y$ and $\overline{EK} \approx (\overline{EK})_x = \overline{EK_0} + (\overline{K_0K})_x$. In addition to this simplification, by taking into account that angle φ is small, we derive an approximate expressions for the spring strain:

$$f_x = u + \varphi\overline{KB}sin\gamma = u + (y_B - y_K)_0 \cdot \varphi,$$
$$f_y = w - \varphi\overline{KB}cos\gamma = w - (x_B - x_K)_0 \cdot \varphi. \tag{14}$$

Index "0" denotes approximation in close vicinity of the state of equilibrium. Total spring deformation is $f + f_{st}$. Static deformation is determined from the equilibrium conditions of the whole system. Finally, the approximate expression for the potential energy of the system is obtained as:

$$E_p \approx \frac{1}{2}k_1p^2 + \frac{1}{2}k_2p^2 + \frac{1}{2}k_{3x}(u + (y_B - y_{K3})_0 \cdot \varphi)^2 + \frac{1}{2}k_{3y}(w - (x_B - x_{K3})_0 \cdot \varphi)^2$$
$$+ \frac{1}{2}k_{4x}(u + (y_B - y_{K4})_0 \cdot \varphi)^2 + \frac{1}{2}k_{4y}(w - (x_B - x_{K4})_0 \cdot \varphi)^2. \tag{15}$$

Taking into account that the corresponding stiffness are the same, i.e. $k_1 = k_2 = k, k_{3x} = k_{4x} = k_x, k_{3y} = k_{4y} = k_y$, we finally obtain:

$$E_p \approx kp^2 + k_xu^2 + k_yw^2 + k_x[(y_B - y_{K3})_0 + (y_B - y_{K4})_0]u\varphi + k_y[(x_{K3} - x_B)_0 + (x_{K4} - x_B)_0]w\varphi$$
$$+ \frac{k_x}{2}[(y_B - y_{K3})_0^2 + (y_B - y_{K4})_0^2]\varphi^2 + \frac{k_y}{2}[(x_{K3} - x_B)_0^2 + (x_{K4} - x_B)_0^2]\varphi^2. \tag{16}$$

3.2. Kinetic energy of the system

The kinetic energy must be a positive definite quadratic form like the potential energy. However, unlike the potential energy, it is not necessary to look for the expression for kinetic energy at an arbitrary position. An approximate expression for kinetic energy of the system is identical to the one due to a motion about the equilibrium point during linear oscillations. It must be mentioned that the kinetic energy of the system becomes a function of generalized velocities only, but not of the generalized coordinates.

Kinetic energy of the system is the sum of kinetic energy of the conveyor base and kinetic energy of the vibratory trough together with an elastic holder. Both of these parts perform linear motion and according to König's theorem, the kinetic energy will be [26–28]:

$$E_k = \frac{1}{2}m_Bv_B^2 + \frac{1}{2}J_B\varphi^2 + \frac{1}{2}m_Kv_C^2 + \frac{1}{2}J_C\varphi^2. \tag{17}$$

Herein, the following notation is used: m_B – mass of the base, v_B – velocity of the COM of the base, m_K – mass of the vibratory trough together with an elastic holder , v_C – velocity of the COM of the trough and the elastic holder, J_B and J_C – moments of inertia of the base and the trough together with the elastic holder relative to the axis perpendicular to Oxy plane passing through the COM, respectively. Fig. 5 shows all speed components $\vec{v}_B$ and $\vec{v}_C$. Velocity vector for the COM of the base is $\vec{v}_B = \dot{u}\vec{i} + \dot{w}\vec{j}$.

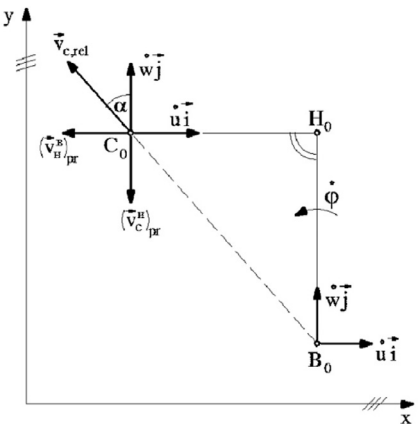

Fig. 5. Speed components $\vec{v}_B$ and $\vec{v}_C$ when the system passes through equilibrium.

The vibratory trough and the elastic holder perform a complex motion. Translational motion is the base displacement, and the relative motion with respect to the base is linear displacement defined by the generalized coordinate p. This means the following:

$$\vec{v}_C = \vec{v}_{C,pr} + \vec{v}_{C,rel}. \tag{18}$$

Where: $\vec{v}_{C,pr}$, denotes translational velocity and $\vec{v}_{C,rel}$–relative velocity. The relative velocity of point C is $v_{C,rel} = \dot{p}$. In order to find the translational velocity, it is assumed that points C and H are fixed to the base. Then, it can be written:

$$\vec{v}_{C,pr} = \vec{v}_B + \left(\vec{v}_H^B\right)_{pr} + \left(\vec{v}_C^H\right)_{pr}. \tag{19}$$

Where the following holds:

$$\left(\vec{v}_H^B\right)_{pr} = -\overline{CB}\dot{\varphi}cos\alpha\vec{i}, \tag{20}$$

and:

$$\left(\vec{v}_C^H\right)_{pr} = -\overline{CB}\dot{\varphi}sin\alpha\,\vec{j}. \tag{21}$$

Relative velocity of the COM of the vibrating through, labeled by C is:

$$\vec{v}_{C,rel} = -\dot{p}sin\alpha\vec{i} + \dot{p}cos\alpha\,\vec{j}. \tag{22}$$

Expression for the squared magnitude of velocity v_C is then:

$$v_C^2 = \dot{p}^2 + \left(\dot{u} - \overline{CB}\dot{\varphi}cos\alpha - \dot{p}sin\alpha\right)^2 + \left(\dot{w} - \overline{CB}\dot{\varphi}sin\alpha + \dot{p}cos\alpha\right)^2. \tag{23}$$

Distance between the centers of inertia of the vibrating trough together with elastic holder and the base in equilibrium is given by:

$$\overline{CB} = \sqrt{(x_{B,0} - x_{C,0})^2 + (y_{C,0} - y_{B,0})^2}. \tag{24}$$

The following geometric relations are also true:

$$y_{C,0} - y_{B,0} = \overline{CB}cos\alpha, \tag{25}$$

$$x_{B,0} - x_{C,0} = \overline{CB}sin\alpha. \tag{26}$$

After squaring appropriate the terms in Eq. (23), by taking into account Eqs. (24) and (26), and suitable arranging, the squared magnitude of velocity v_C, as function of the generalized coordinates (p, u, w, φ), including geometric parameters of the system, is obtained in the final form:

$$\begin{aligned} v_C^2 = {} & \dot{p}^2 + \dot{u}^2 + \dot{w}^2 + \dot{\varphi}^2\left[(x_{B,0} - x_{C,0})^2 + (y_{C,0} - y_{B,0})^2\right] - 2\dot{u}\dot{\varphi}(y_{C,0} - y_{B,0}) - 2\dot{w}\dot{\varphi}(x_{B,0} - x_{C,0}) \\ & + 2\dot{p}\dot{w}cos\alpha - 2\dot{p}\dot{u}sin\alpha + 2\dot{p}\dot{\varphi}[(y_{C,0} - y_{B,0})sin\alpha - (x_{B,0} - x_{C,0})cos\alpha]. \end{aligned} \tag{27}$$

Finally, from Eqs. (17) and (27), the final expression for the kinetic energy of the system is:

$$\begin{aligned} E_k \approx {} & \frac{1}{2}m_K\dot{p}^2 + \frac{1}{2}(m_K + m_B)\dot{u}^2 + \frac{1}{2}(m_K + m_B)\dot{w}^2 + \frac{1}{2}\left\{J_C + J_B + 2m_K\left[(x_{B,0} - x_{C,0})^2 + (y_{B,0} - y_{C,0})^2\right]\right\}\dot{\varphi}^2 \\ & - m_K(y_{C,0} - y_{B,0})\dot{u}\dot{\varphi} - m_K(x_{B,0} - x_{C,0})\dot{w}\dot{\varphi} + m_K\dot{p}\dot{w}cos\alpha - m_K\dot{p}\dot{u}sin\alpha \\ & + m_K[(y_{C,0} - y_{B,0})sin\alpha - (x_{B,0} - x_{C,0})cos\alpha]\dot{p}\dot{\varphi}. \end{aligned} \tag{28}$$

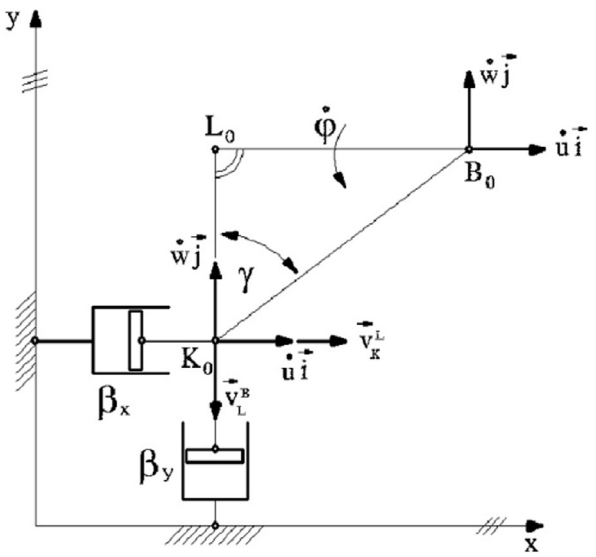

Fig. 6. The component of velocity $\vec{v}_K$ when the system passes through equilibrium.

3.3. Dissipative (Rayleigh) function

In addition to the potential forces, resistance forces also affect the behavior of the considered mechanical system. The portion of non-potential generalized forces Q_j represents the generalized resistance forces Q_{wj}. The damping-generalized forces can be expressed as:

$$Q_{wj} = -\frac{\partial \Phi}{\partial q_j}, \tag{29}$$

where Φ is dissipative function of the system.

In order to obtain generalized damping forces of a linear system, the dissipative function has to be approximated by a quadratic form having constant coefficients:

$$\Phi \approx \frac{1}{2}\sum_{i=1}^{s}\sum_{j=1}^{s} b_{ij}\dot{q}_i\dot{q}_j. \tag{30}$$

Damping forces appear in the elastic holders comprising of the elastic-damping coupling elements ((5) in Fig. 1) and damping shock absorbers ((2) in Fig. 1). Both elastic-damping elements are the same and have the same damping coefficients β. Therefore, dissipative function of these two elements, is $\Phi_1 = \beta\dot{p}^2$. Dissipative function for the damping shock absorbers is dependent on the relative velocity of the pistons with respect to the cylinders, but only when passing through the equilibrium state occurs [25–28].

The piston velocity is the component in the direction of the shock absorber. All components of the velocity at point K are depicted in Fig. 6. The base performs straight motion so that:

$$\vec{v}_K = \vec{v}_B + \vec{v}_L^B + \vec{v}_K^L. \tag{31}$$

It can be seen from Fig. 6 that the following holds:

$$v_L^B = (x_B - x_K)_0 \cdot \dot{\varphi}, \tag{32}$$

$$v_K^L = (y_B - y_K)_0 \cdot \dot{\varphi}. \tag{33}$$

Velocity of the horizontal shock absorber is equal to the horizontal velocity component at point K. Also, velocity of the movable part of the shock absorber is relative velocity of the movable part with respect to the stationary part, so:

$$v_{rel,x} = \dot{u} + (y_B - y_K)_0 \cdot \dot{\varphi}. \tag{34}$$

Similarly, relative velocity of the movable part with respect to the stationary part of the vertical shock absorber is equal to the vertical component of velocity at point K, i.e.:

$$v_{rel,y} = \dot{w} - (x_B - x_K)_0 \cdot \dot{\varphi}. \tag{35}$$

Both horizontal shock absorbers have damping coefficient β_x while the vertical shock absorbers have damping coefficient β_y. Now we can write the expression for the dissipating function:

$$\Phi \approx \beta\dot{p}^2 + \frac{1}{2}\beta_x(\dot{u} + (y_B - y_{K3})_0 \cdot \dot{\varphi})^2 + \frac{1}{2}\beta_y(\dot{w} - (x_B - x_{K3})_0 \cdot \dot{\varphi})^2 + \frac{1}{2}\beta_x(\dot{u} + (y_b - y_{K4})_0 \cdot \dot{\varphi})^2 + \frac{1}{2}\beta_y(\dot{w} - (x_B - x_{K4})_0 \cdot \dot{\varphi})^2. \tag{36}$$

3.4. The generalized driving force

The second part of the non-potential generalized forces comes from the excitation force $\vec{F}$. To determine the generalized excitation force it is necessary to determine its virtual work. This virtual work is $\delta A_\Omega = F\delta p$. On the other hand, this virtual work is $\delta A_\Omega = \underline{Q}_\Omega^T \delta\underline{q}$. Thus, the vector of generalized excitation force in this case is: $\underline{Q}_\Omega^T = [F, 0, 0, 0]^T$.

The damping and excitation forces affect behavior of the system besides potential force. Lagrange equations of the second kind for a linear system are [25–28]:

$$\frac{d}{dt}\left(\frac{\partial E_k}{\partial \dot{q}_j}\right) + \frac{\partial \Phi}{\partial \dot{q}_j} + \frac{\partial E_p}{\partial q_j} = Q_{\Omega j}(j = 1, 2, ..., 4). \tag{37}$$

Let us derive expressions for particular partial derivatives comprising the Lagrange equation of the linear system. From Eq. (28), partial derivatives of kinetic energy E_K in terms of the state variables $\dot{q}_j$ can be obtained:

$$\frac{\partial E_k}{\partial \dot{p}} = m_K\dot{p} + m_K\dot{w}cos\alpha - m_K\dot{u}sin\alpha + m_K[(y_{C,0} - y_{B,0})sin\alpha - (x_{B,0} - x_{C,0})cos\alpha]\dot{\varphi}, \tag{38}$$

$$\frac{\partial E_k}{\partial \dot{u}} = (m_K + m_B)\dot{u} - m_K(y_{C,0} - y_{B,0})\dot{\varphi} - m_K\dot{p}sin\alpha, \tag{39}$$

$$\frac{\partial E_k}{\partial \dot{w}} = (m_K + m_B)\dot{w} - m_K(x_{B,0} - x_{C,0})\dot{\varphi} + m_K\dot{p}cos\alpha, \tag{40}$$

$$\frac{\partial E_k}{\partial \dot{\varphi}} = \left\{J_C + J_B + 2m_K\left[(x_{B,0} - x_{C,0})^2 + (y_{B,0} - y_{C,0})^2\right]\right\}\dot{\varphi} - m_K(y_{C,0} - y_{B,0})\dot{u} - m_K(x_{B,0} - x_{C,0})\dot{w} + m_K[(y_{C,0} - y_{B,0})sin\alpha - (x_{B,0} - x_{C,0})cos\alpha]\dot{p}. \tag{41}$$

Time derivatives of the previously calculated partial derivatives are given by:

$$\frac{d}{dt}\left(\frac{\partial E_k}{\partial \dot{p}}\right) = m_K\ddot{p} + (m_Kcos\alpha)\ddot{w} - (m_Ksin\alpha)\ddot{u} + m_K[(y_{C,0} - y_{B,0})sin\alpha - (x_{B,0} - x_{C,0})cos\alpha]\ddot{\varphi}, \tag{42}$$

$$\frac{d}{dt}\left(\frac{\partial E_k}{\partial \dot{u}}\right) = (m_K + m_B)\ddot{u} - m_K(y_{C,0} - y_{B,0})\ddot{\varphi} - (m_Ksin\alpha)\ddot{p}, \tag{43}$$

$$\frac{d}{dt}\left(\frac{\partial E_k}{\partial \dot{w}}\right) = (m_K + m_B)\ddot{w} - m_K(x_{B,0} - x_{C,0})\ddot{\varphi} + (m_Kcos\alpha)\ddot{p}, \tag{44}$$

$$\frac{d}{dt}\left(\frac{\partial E_k}{\partial \dot{\varphi}}\right) = \left\{J_C + J_B + 2m_K\left[(x_{B,0} - x_{C,0})^2 + (y_{B,0} - y_{C,0})^2\right]\right\}\ddot{\varphi} - m_K(y_{C,0} - y_{B,0})\ddot{u} - m_K(x_{B,0} - x_{C,0})\ddot{w} + m_K[(y_{C,0} - y_{B,0})sin\alpha - (x_{B,0} - x_{C,0})cos\alpha]\ddot{p}. \tag{45}$$

From Eq. (36) we derive partial derivatives of dissipative function in terms of the state variables $\dot{q}_j$:

$$\frac{\partial \Phi}{\partial \dot{p}} = 2\beta\dot{p}, \tag{46}$$

$$\frac{\partial \Phi}{\partial \dot{u}} = 2\beta_x\dot{u} + \beta_x[(y_B - y_{K3})_0 + (y_B - y_{K4})]\dot{\varphi}, \tag{47}$$

$$\frac{\partial \Phi}{\partial \dot{w}} = 2\beta_y\dot{w} + \beta_y[-(x_B - x_{K3})_0 - (x_B - x_{K4})_0]\dot{\varphi}, \tag{48}$$

$$\frac{\partial \Phi}{\partial \dot{\varphi}} = \beta_x[(y_B - y_{K3})_0 + (y_B - y_{K4})_0]\dot{u} + \beta_y\varphi[(x_{K3} - x_B)_0 + (x_{K4} - x_B)_0]\dot{w} + \left[\beta_x\left((y_B - y_{K3})_0^2 + (y_B - y_{K4})_0^2\right) + \beta_y\left((x_B - x_{K3})_0^2 + (x_B - x_{K4})_0^2\right)\right]\dot{\varphi}. \tag{49}$$

From Eq. (16) we can obtain partial derivatives of the potential energy Ep in terms of the state variables q_j:

$$\frac{\partial E_p}{\partial p} = 2kp, \tag{50}$$

$$\frac{\partial E_p}{\partial u} = 2k_x u + k_x[(y_B - y_{K3})_0 + (y_B - y_{K4})_0]\varphi, \tag{51}$$

$$\frac{\partial E_p}{\partial w} = 2k_y w + k_y[(x_{K3} - x_B)_0 + (x_{K4} - x_B)_0]\varphi, \tag{52}$$

$$\begin{aligned}\frac{\partial E_p}{\partial \varphi} &= \left[k_x\left[(y_B - y_{K3})_0^2 + (y_B - y_{K4})_0^2\right] + k_y\left[(x_{K3} - x_B)_0^2 + (x_{K4} - x_B)_0^2\right]\right]\varphi \\ &\quad + k_x[(y_B - y_{K3})_0 + (y_B - y_{K4})_0]u + k_y[(x_{K3} - x_B)_0 + (x_{K4} - x_B)_0]w.\end{aligned} \tag{53}$$

Finally, by substituting expressions, Eqs. (38)–(53), into Eq. (37) the matrix form of the system equations is obtained:

$$\underline{M}\ddot{\underline{q}} + \underline{B}\dot{\underline{q}} + \underline{K}\underline{q} = \underline{Q}_\Omega. \tag{54}$$

The corresponding matrix terms in this equation are as follows:

I. The inertia matrix

$$\underline{M} = \begin{bmatrix} m_{11} & m_{12} & m_{13} & 0 \\ m_{21} & m_{22} & 0 & m_{24} \\ m_{31} & 0 & m_{33} & m_{34} \\ 0 & m_{42} & m_{43} & m_{44} \end{bmatrix}, \tag{55}$$

where the corresponding coefficients of inertia matrix are:

$$\begin{aligned} m_{11} &= m_K; \\ m_{12} = m_{21} &= -m_K sin\alpha;\ \ m_{13} = m_{31} = m_K cos\alpha; \\ m_{14} = m_{41} &= m_K(y_{C,0} - y_{B,0})sin\alpha + m_K(x_{C,0} - x_{B,0})cos\alpha = 0; \\ m_{22} = m_K + m_B;&\ \ m_{23} = m_{32} = 0;\ \ m_{24} = m_{42} = -m_K(y_{C,0} - y_{B,0}); \\ m_{33} &= m_K + m_B;\ \ m_{34} = m_{43} = m_K(x_K - x_B); \\ m_{44} &= J_C + J_B + m_K\left[(x_{C,0} - x_{B,0})^2 + (y_{C,0} - y_{B,0})^2\right] \end{aligned}$$

II. The damping matrix

$$\underline{B} = \begin{bmatrix} b_{11} & 0 & 0 & 0 \\ 0 & b_{22} & 0 & b_{24} \\ 0 & 0 & b_{33} & b_{34} \\ 0 & b_{42} & b_{43} & b_{44} \end{bmatrix}. \tag{56}$$

Wherein the elements of the matrix are:

$$\begin{aligned} b_{11} = 2\beta;&\ \ b_{12} = b_{21} = 0;\ \ b_{13} = b_{31} = 0;\ \ b_{14} = b_{41} = 0; \\ b_{22} = 2\beta_x;&\ \ b_{23} = b_{32} = 0;\ \ b_{24} = b_{42} = \beta_x[(y_B - y_{K3})_0 + (y_B - y_{K4})_0]; \\ b_{33} &= 2\beta_y;\ \ b_{34} = b_{43} = \beta_y[(x_{K3} - x_B)_0 + (x_{K4} - x_B)_0]; \\ b_{44} &= \beta_x\left[(y_B - y_{K3})_0^2 + (y_B - y_{K4})_0^2\right] + \beta_y\left[(x_B - x_{K3})_0^2 + (x_B - x_{K4})_0^2\right] \end{aligned}$$

III. The stiffness matrix:

$$\underline{K} = \begin{bmatrix} k_{11} & 0 & 0 & 0 \\ 0 & k_{22} & 0 & k_{24} \\ 0 & 0 & k_{33} & k_{34} \\ 0 & k_{42} & k_{43} & k_{44} \end{bmatrix}. \tag{57}$$

Wherein the elements of the matrix are:

$$\begin{aligned} k_{11} &= 2k; \\ k_{12} = k_{21} = k_{13} = k_{31} &= k_{14} = k_{41} = 0; \\ k_{22} = 2k_x;&\ \ k_{23} = k_{32} = 0;\ \ k_{24} = k_{42} = k_x[(y_B - y_{K3})_0 + (y_B - y_{K4})_0]; \\ k_{33} &= 2k_y;\ \ k_{34} = k_{43} = k_y[(x_{K3} - x_B)_0 + (x_{K4} - x_B)_0]; \\ k_{44} &= k_x\left[(y_B - y_{K3})_0^2 + (y_B - y_{K4})_0^2\right] + k_y\left[(x_{K3} - x_B)_0^2 + (x_{K4} - x_B)_0^2\right] \end{aligned}$$

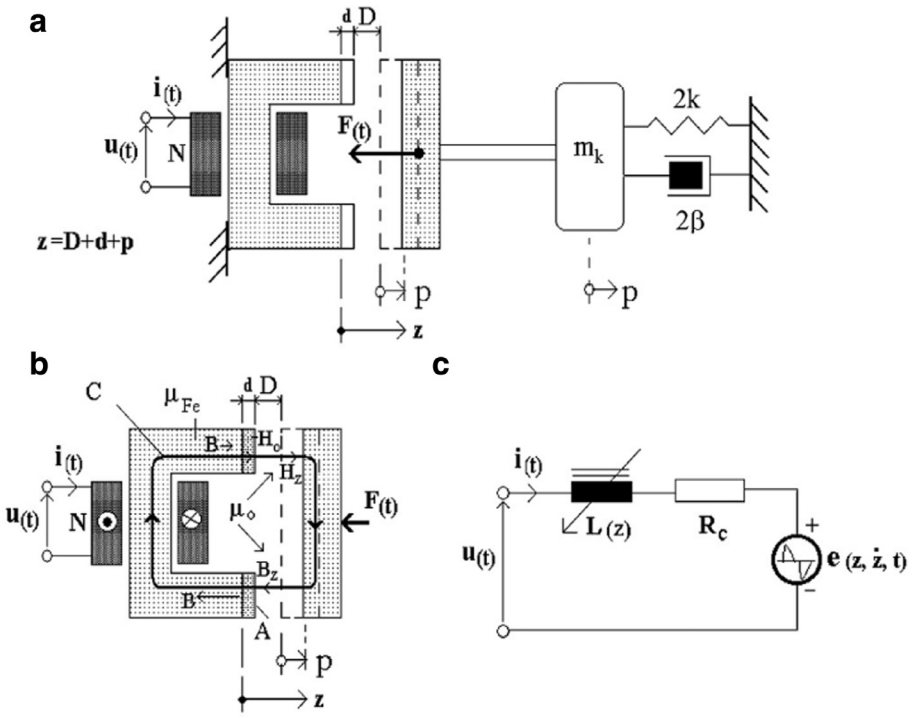

Fig. 7. Functional model of the EVA; (a) – electromechanical model, (b) – magnetic circuit, (c) – equivalent electric circuit.

External force acting on the system:

$$\underline{Q}_{\Omega} = \begin{bmatrix} -F \\ 0 \\ 0 \\ 0 \end{bmatrix}, \tag{58}$$

and the system states:

$$\underline{q} = \begin{bmatrix} p \\ u \\ w \\ \varphi \end{bmatrix}. \tag{59}$$

All major minors of the stiffness matrix K are positive, as can be seen from Eq. (57), meaning that Sylvester criterion [27,28] is satisfied. It represents a necessary and sufficient condition for stability of the equilibrium state, and while the eventual oscillations are possible.

4. The electromagnetic actuator as a source of excitation force

The dynamic model of vibratory conveyor described above contains one excitation source which is represented by the electromagnetic force $\vec{F}$. This force is the result of electromechanical energy conversion in the electromagnetic actuator, which can be justifiably called the force excitation generator. This excitation force acts in the direction of generalized coordinate p and it is dependent on the excitation current in EVA and size of the air gap between the inductor and armature (i.e. anchor). Since the electromagnetic actuator is an electromechanical system that constitutes a unified whole within the mechanical vibratory conveyor (Fig. 7), in order to correctly represent the entire system it is necessary to describe the electrical and mechanical phenomena in it.

Electromechanical functional model of the actuator within the vibratory system is given in Fig. 7(a). Before deriving the electro-mechanical dynamic model of EVA, certain assumptions will be introduced. Distance between the fixed inductor and movable armature (anchor) at equilibrium is denoted by D. Generalized coordinate axis is denoted by p according to the direction shown in Fig. 7(a). It is assumed that iron core of the inductor is made of laminated thin plates of permeability μ_{Fe} which is an order of magnitude greater than the magnetic permeability of the air gap μ_0. Permeability of the bronze pole extensions of thickness d is equal to permeability of the air. This bronze disc (pole cover) does not allow armature to form a closed iron magnetic circuit, i.e. it prevents "sticking". The edge effects of the magnetic circuit (dissipation) in the

actuator and losses due to eddy currents are neglected. The effective area enclosed by the total magnetic flux is labeled by A. In order to make simplification in EVA analysis, it is assumed that base oscillations in the u and w directions are negligible relative to the oscillations in the p direction. It is also assumed that mass of the base of the vibratory conveyor is significantly lower than the mass of the movable vibratory through including the armature (anchor) of EVA, [8].

By applying Ampere's law for contour C of the actuator magnetic circuit (Fig. 7(b)) one obtains:

$$\oint_C \vec{H}d\vec{l} = \int_S \vec{J}d\vec{S}. \tag{60}$$

It is possible to write Eq. (60) in the following form:

$$2H_z(D+p) + 2H_b d = Ni, \tag{61}$$

where the following notation is used: H_z, H_b – magnetic fields in the air gap and bronze, respectively, N – the number of inductor windings in the actuator of total resistance R_c. The coil is connected to a voltage source, while the current flowing through the coil is labeled by i. According to the right hand rule, the total Ampere-turns Ni existing in the area containing the contour C has a positive sign–Ampere's law. Due to significantly higher permeability of iron, it has been assumed that the magnetic field in iron is negligible compared to the one in the air gap and bronze. The magnetic field induction is:

$$B = \mu_0 H_z = \mu_0 H_b. \tag{62}$$

Substituting this expression into Eq. (61), we obtain the following expression for induction:

$$B = \frac{\mu_0 Ni}{2(D+d+p)}. \tag{63}$$

Magnetic flux in the air gap and bronze is:

$$\Phi_S = \int_S \vec{B}d\vec{S}. \tag{64}$$

This magnetic flux through surface A of the pole end is:

$$\Phi_A = \frac{\mu_0 NAi}{2(D+d+p)}. \tag{65}$$

The total magnetic flux is:

$$\lambda(\dot{q}, p) = N\Phi_A = \frac{\mu_0 N^2 Ai}{2(D+d+p)}. \tag{66}$$

The state function of magnetic co-energy is:

$$W_m^* = \int_0^i \lambda(i, p)di. \tag{67}$$

After substituting Eq. (66) for total flux λ into Eq. (67), the following expression is obtained:

$$W_m^*(i, p) = \int_0^i \frac{\mu_0 N^2 Ai}{2(D+d+p)}di. \tag{68}$$

When the integral in Eq. (68) is solved, the state function of magnetic co-energy is obtained:
When this integral is solved over the variable i, the function of the state of magnetic co-energy is obtaining:

$$W_m^*(i, p) = \frac{\mu_0 N^2 Ai^2}{4(D+d+p)}. \tag{69}$$

By using generally known relation [25,26,28] the electromagnetic force is easily calculated from the functions of the magnetic co-energy:

$$F = -\frac{\partial W_m^*(i, p)}{\partial p}. \tag{70}$$

From Eqs. (69) and (70) the electromagnetic force generated in the actuator is obtained:

$$F = \frac{\mu_0 N^2 Ai^2}{4(D+d+p)^2}. \tag{71}$$

The resulting expression may be presented in a more convenient form [26]:

$$F = \frac{a_i i^2}{(D+d+p)^2}, \tag{72}$$

where constant a_i referring to characteristics of the inductor and magnetic circuit of the actuator is given by the relation:

$$a_i = \frac{\mu_0 N^2 A}{4}. \tag{73}$$

By using the mechanical model shown in Fig. 7(a) and Eq. (72), it is possible to derive the equation of motion of the system in the direction of relative coordinate p in the form:

$$m_k \ddot{p} + 2\beta\dot{p} + 2kp \approx -\frac{a_i i^2}{(D+d+p)^2}. \tag{74}$$

The sign "−" in the dynamic equation implies that the force is in the opposite direction of the indicated direction of growing values of relative coordinates.

To obtain the equation of electrical behavior of the actuator, it is necessary to form Lagrangian of the electromechanical subsystem shown in Fig. 7. Therefore, it can be written:

$$\Im_1^e(\dot{p}, p, i) \approx \frac{1}{2} m_k \dot{p}^2 + \frac{a_i i^2}{(D+d+p)} - \frac{1}{2} 2kp^2. \tag{75}$$

Rayleigh dissipative function of the considered subsystem can be represented by [25,26,28]:

$$\Re_1^e(\dot{p}, i) = \frac{1}{2} 2\beta\dot{p}^2 + \frac{1}{2} R_c i^2. \tag{76}$$

The equation of motion for the electromagnetic subsystem is obtained [25,26,28] as:

$$\frac{d}{dt}\left[\frac{\partial \Im_1^e(\dot{p}, p, i)}{\partial i}\right] + \frac{\partial \Re_1^e(\dot{p}, i)}{\partial i} = u(t). \tag{77}$$

The terms for individual partial derivatives are:

$$\frac{d}{dt}\left[\frac{\partial \Im_1^e(\dot{p}, p, i)}{\partial i}\right] = \frac{d}{dt}\left[\frac{2a_i i}{D+d+p}\right] = \frac{2a_i \frac{di}{dt}}{D+d+p} - \frac{2a_i i\dot{p}}{(D+d+p)^2}, \tag{78}$$

$$\frac{\partial \Re_1^e(\dot{p}, i)}{\partial i} = R_c i. \tag{79}$$

The equation of motion for the electromagnetic subsystem is obtained from Eq. (77):

$$\frac{2a_i}{D+d+p}\frac{di}{dt} + R_c i - \frac{2a_i i\dot{p}}{(D+d+p)^2} = u(t). \tag{80}$$

Term $D+d+p$ in Eqs. (78)–(80) is variable and represents size of the air gap z in an actuator magnetic circuit, as indicated in Fig. 7(a) and (b). Eq. (80) can be written in the final form as a function of the variable z as:

$$\frac{2a}{z}\frac{di}{dt} + R_c i - \frac{2a_i i\dot{z}}{z^2} = u(t), \tag{81}$$

and respectively,

$$L(z)\frac{di}{dt} + R_c i + e(\dot{z}, z, t) = u(t), \tag{82}$$

where the following notation is used:

$L(z) = 2a_i/z$	is inductance of the electromagnetic actuator,
R_c	is electrical resistance of inductor coil of the EVA,
$e(\dot{z}, z, t) = -2a_i i\dot{z}/z^2$	is induced counter-electromotive force (CEMF)

On the basis of this consideration, the equivalent circuit of the EVA is proposed and shown in Fig. 7(c).

5. Verification of the mathematical model of vibratory conveyor

5.1. The simulation model

Eq. (54) can be written in the form:

$$\ddot{\underline{q}} = -\underline{M}^{-1}\underline{B}\dot{\underline{q}} - \underline{M}^{-1}\underline{K}\underline{q} + \underline{M}^{-1}\underline{Q}_\Omega. \tag{83}$$

If the system state is adopted to be $\tilde{x} = [\dot{\underline{q}}\ \underline{q}]^T$, system input $\tilde{u} = \underline{F}$, and system output $\tilde{y} = \underline{q}$, the state-space model of system will be:

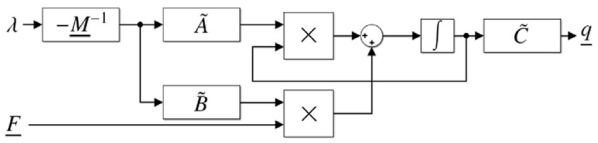

Fig. 8. The simulation block scheme.

$$\dot{\tilde{x}} = \tilde{A}\tilde{x} + \tilde{B}\tilde{u},$$
$$\tilde{y} = \tilde{C}\tilde{x}. \tag{84}$$

Wherein the corresponding matrices are given by:

$$\tilde{A} = \begin{bmatrix} -\underline{M}^{-1}\underline{B} & -\underline{M}^{-1}\underline{K} \\ I & 0 \end{bmatrix}_{8x8}, \tag{85}$$

$$\tilde{B} = \begin{bmatrix} \underline{M}^{-1} \\ 0 \end{bmatrix}_{8x1}, \tag{86}$$

$$\tilde{C} = [0\ \ I]_{4x8}. \tag{87}$$

The simulation block scheme is given in Fig. 8.

System inputs F and λ_t are the external force and dimensionless correction coefficient, respectively. Statistically, during operation of the vibratory conveying, one part of the particles is on the vibratory trough, and another part of the particles is in the bounce. The bouncing particles, or those that are not in contact with the vibratory through, do not affect the load mass of the conveyor. The vibratory regime of the conveyor is determined by coefficient K ($\sim \ddot{p}_{max}/g$, g is gravitational acceleration=9.81 m/s^2), which determines the quantity of bouncing particles, [1].

The load mass of the conveying material has to be reduced by coefficient λ_t, so the total load mass is given by Eq. (88).

$$m_k = m_{k0} + \lambda_t \Delta m_k. \tag{88}$$

In practice, the empirical correction coefficient λ_t is determined on the basis of its relation to the ratio K of the vibratory conveyor [1]. For the real range of values of coefficient K of vibratory conveyors, $3.3 > K > 1$, value of the correction coefficient λ_t is within the range $0.6 > \lambda_t > 0.1$. Since mass m_{k0} is unchangeable, it is concluded that the change of λ_t leads to changing of the total oscillating mass m_k, Eq. (88).

The system output is $\underline{q} = [p\ u\ w\ \varphi]^T$.

The excitation force, generated by thyristor converter [8–11], is given by Eq. (89):

$$F(t) = k_i i^2(t), \tag{89}$$

where:

k_i –current gain of the actuator ($= a_i/(D+d)^2$), where p is assumed to be zero for $t = 0+$.

Input voltage (mains voltage) of the thyristor converter is:

$$u(t) = \sqrt{2}U sin(\omega t). \tag{90}$$

By applying an appropriate phase angle control (PAC), EVA current is [29,30]:

$$i(t) = \frac{\sqrt{2}U}{\sqrt{R_c^2 + (\omega L(z))^2}}\left[sin(\omega t - \theta) - e^{\frac{\alpha^*}{\omega\tau}} e^{-\frac{t}{\tau}} sin(\alpha^* - \theta)\right], \tag{91}$$

where:

R_c	is electrical resistance of inductor coil of the EVA,
$L(z)$	is actuator inductance; $L(z) = 2a_i/(D+d+p)$,
$L(0)$	is actuator inductance in equilibrium position; $L(0) = 2a_i/(D+d)$,
ω	is angular frequency ($\omega = 2\pi f$), where f is mains frequency of 50 Hz),
α^*	is phase angle, and
$\tau = L(z)/R_c$	is electrical time constant of the EVA coil.

One current impulse (force impulse) is used for excitation of vibratory conveyor's oscillatory modes which corresponds to Dirac excitation. Unidirectional thyristor converter [8,11] is used for obtaining such an impulse. Inductive resistance of EVA inductor is significantly larger compared to its ohmic resistance ($\omega L(0) \gg R_c$).

As regards control range of the thyristor converter, α^* must satisfy the following condition [30]:

$$\theta \le \alpha^* < \pi. \tag{92}$$

Where θ is given by:

$$\theta = arctg\left(\frac{\omega L(0)}{R_c}\right). \tag{93}$$

Table 1
Simulation parameters.

Coordinates of the base COM	$B[x_B = 194\,\text{mm}$ and $y_B = 89\,\text{mm}]$
Coordinates of the vibratory trough COM	$C[x_C = 92\,\text{mm}$ and $y_C = 129\,\text{mm}]$
Distance from COM of the vibratory trough (point C) to COM of the base (point B)	$r = 110\,mm$
K_3 coordinates	$K_3[x_3 = 33\,\text{mm}\ y_3 = 15\,\text{mm}]$
K_4 coordinates	$K_4[x_4 = 211.83\,\text{mm}\ y_4 = 15\,\text{mm}]$
$\overline{K_3B}$ and $\overline{K_4B}$ distances	$r_3 = 177\,\text{mm}$ and $r_4 = 76\,\text{mm}$
Inclination angle of the supporting springs	$\alpha = 70^\circ$
Characteristic geometric angles	$\gamma_3 = 65.4^\circ$ and $\gamma_4 = 13.6^\circ$
Mass of the empty vibratory trough	$m_{k0} = 0.83\,\text{kg}$
Total mass of the filled vibratory trough	$m_k = m_{k0} + \lambda_t \Delta m_K$
Mass of the conveying material	$\Delta m_k = \rho_{material}(\text{g/cm}^3)V_k(\text{cm}^3) = 380\rho_{material}(\text{g/cm}^3)$
Volume of the vibratory trough	$V_k = 269\,\text{cm}^3$
Correction coefficient λ_t	$0.6 > \lambda_t > 0.1$
Mass of the conveyor's base	$m_b = 4\,\text{kg}$
Total moment of inertia of the empty trough together with the holder and the actuator's anchor	$J_{k0} = 3.86 \cdot 10^{-3}\,\text{kgm}^2$
Moment of inertia of the base	$J_b = 0.017\,\text{kgm}^2$
Stiffness of the supporting elastic elements	$k_1 = k_2 = 0.43 \cdot 10^5\,\text{N/m}$
Stiffness of damping elements in the horizontal direction	$k_{3x} = k_{4x} = k_x = 0.08 \cdot 10^5\,\text{N/m}$
Stiffness of damping elements in the vertical direction	$k_{3y} = k_{4y} = k_y = 0.4 \cdot 10^5\,\text{N/m}$
Total damping of the supporting elastic elements	$\beta_1 = \beta_2 = \beta = 1.2\,\text{N/m/s}$
Damping of the damping elements in the horizontal direction	$\beta_{3x} = \beta_{4x} = \beta_x = 0.1\,\text{N/m/s}$
Damping of the damping elements in the vertical direction	$\beta_{3y} = \beta_{4y} = \beta_y = 0.5\,\text{N/m/s}$
Distance between the anchor and inductor at equilibrium	$D = 6\,\text{mm}$
Width of the pole cover	$d = 0.5\,\text{mm}$
Inductance of EVA coil at equilibrium	$L(0) = 1.6\,\text{H}$
Electrical resistance of EVA coil	$R_c = 92\,\Omega$
Actual value of source voltage	$u(t) = U\sqrt{2}\sin(2\pi ft); U = 440V,\ \ f = 50\,\text{Hz}$

5.2. The simulation results

This section presents the simulation results of the considered electromagnetic vibratory conveyor. The real values of the conveyor mechanical parameters are set in the simulation model. They are given by mathematical expressions in the previous sections on the basis of the actual geometric relations and coordinates of the characteristic points. The electrical parameters corresponding to a real conveyor are also set. The characteristic geometric relations and parameter values are given in Table 1. The implementation of the simulation model and obtaining simulation results were carried out in the simulation program MATLAB/Simulink [31].

In order to examine the behavior of the empty ($\lambda_t = 0$) vibratory conveyor, a simulation has been carried out. At this stage, influence of the quantity and type of the transported material has not been taken into consideration, due to complexity of such analysis. Impulse response of the empty conveyor is shown in Fig. 9. Accelerations of the system are also important, since they can be measured by a real experiment.

The excitation force, determined by Eq. (89), will produce underdamped oscillation of the vibratory conveyor. The effect of a force pulse on conveyor's response can be seen readily in the range $[0, 0.1]$ s, Fig. 10. The frequencies and amplitudes of these damped oscillations can be observed in a short time range.

It can be observed in Figs. 9 and 10, that the amplitudes and frequencies of the simulated signals are reasonable, as will be shown later on in the experiment.

The response of the simulated conveyor and EVA supply immediately after the excitation current pulse are shown in Fig. 11, where EVA voltage and current are obtained by Eqs. (90) and (91), respectively.

5.3. Description of the experimental setup

Schematic block diagram of the system used for experimental verification of the simulation results is shown in Fig. 12. The presented system consists of the four main components: (1) unidirectional thyristor converter for EVA excitation, (2) sensor system for measuring the characteristic quantities, (3) control system based on *PC* 104 platform, and (4) oscilloscope used for capturing signals (oscilloscopic records).

The experimental setup is powered by mains: 230 V, 50 Hz. The step-up autotransformer is supplied by mains voltage via protective fuse *F*1. Furthermore, unidirectional tyristor converter for the EVA excitation is powered by the autotransformer. EVA voltage can be adjusted in the range 0–480 V, 50 Hz. In this case, this voltage is set to 440 V.

The unidirectional power converter consists of one thyristor T_h, driving circuit for its excitation, and the corresponding protection circuits. Thyristor T_h is mounted on a heat sink where a thermal switch is placed to shut down the whole drive unit if temperature of the heat sink is too increased, or overheating of the thyristor occurs. In addition to this, several other

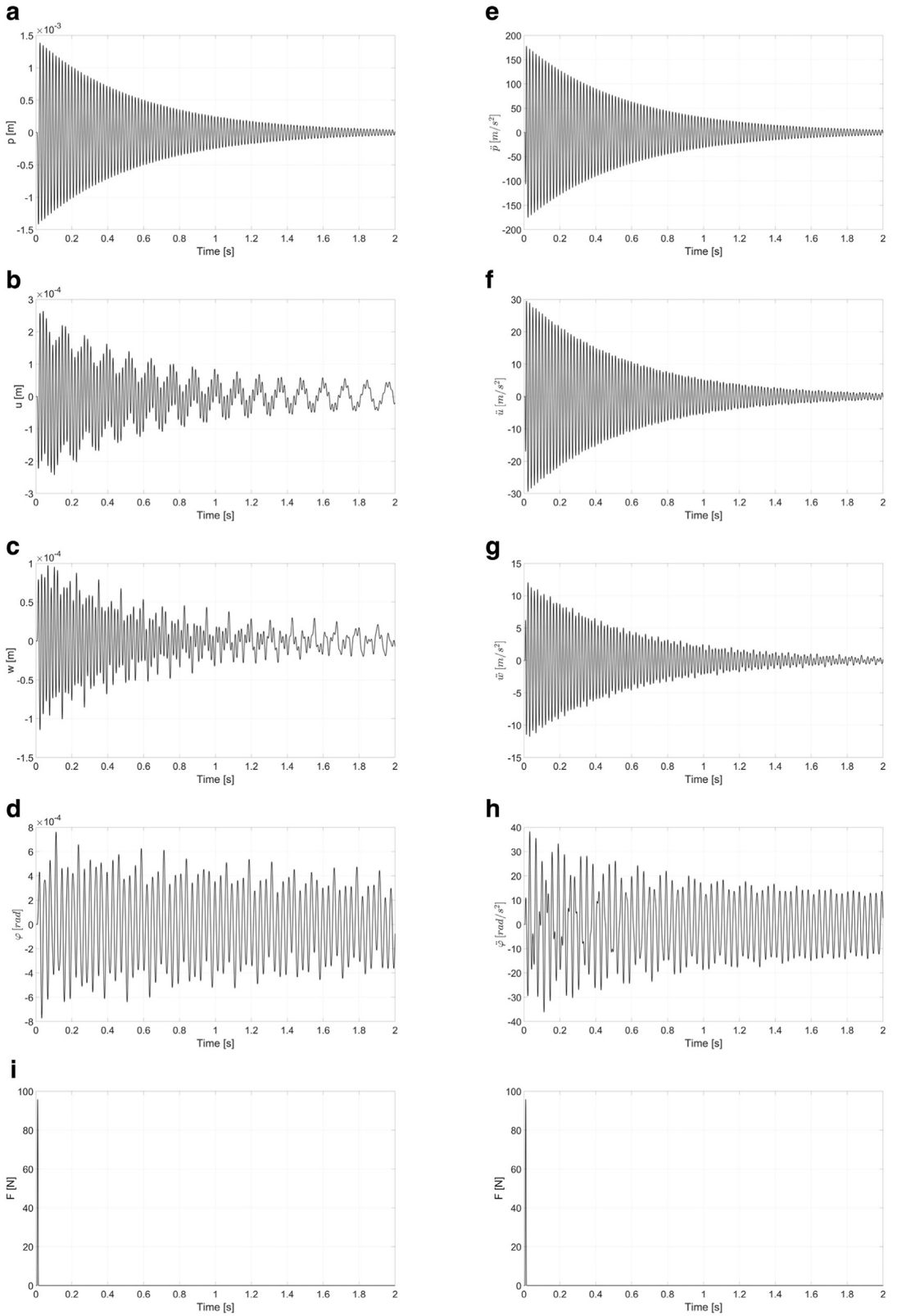

Fig. 9. Responses to impulse excitation of the simulated vibratory conveyor: (a)–displacement p, (b)–displacement u, (c)–displacement v, (d)–deflection (angle of rotation) φ, (e)–acceleration $\ddot{p}$, (f)–acceleration $\ddot{u}$, (g)–acceleration $\ddot{v}$, (h)–acceleration $\ddot{\varphi}$ and (i)–excitation force within time interval [0, 2] s.

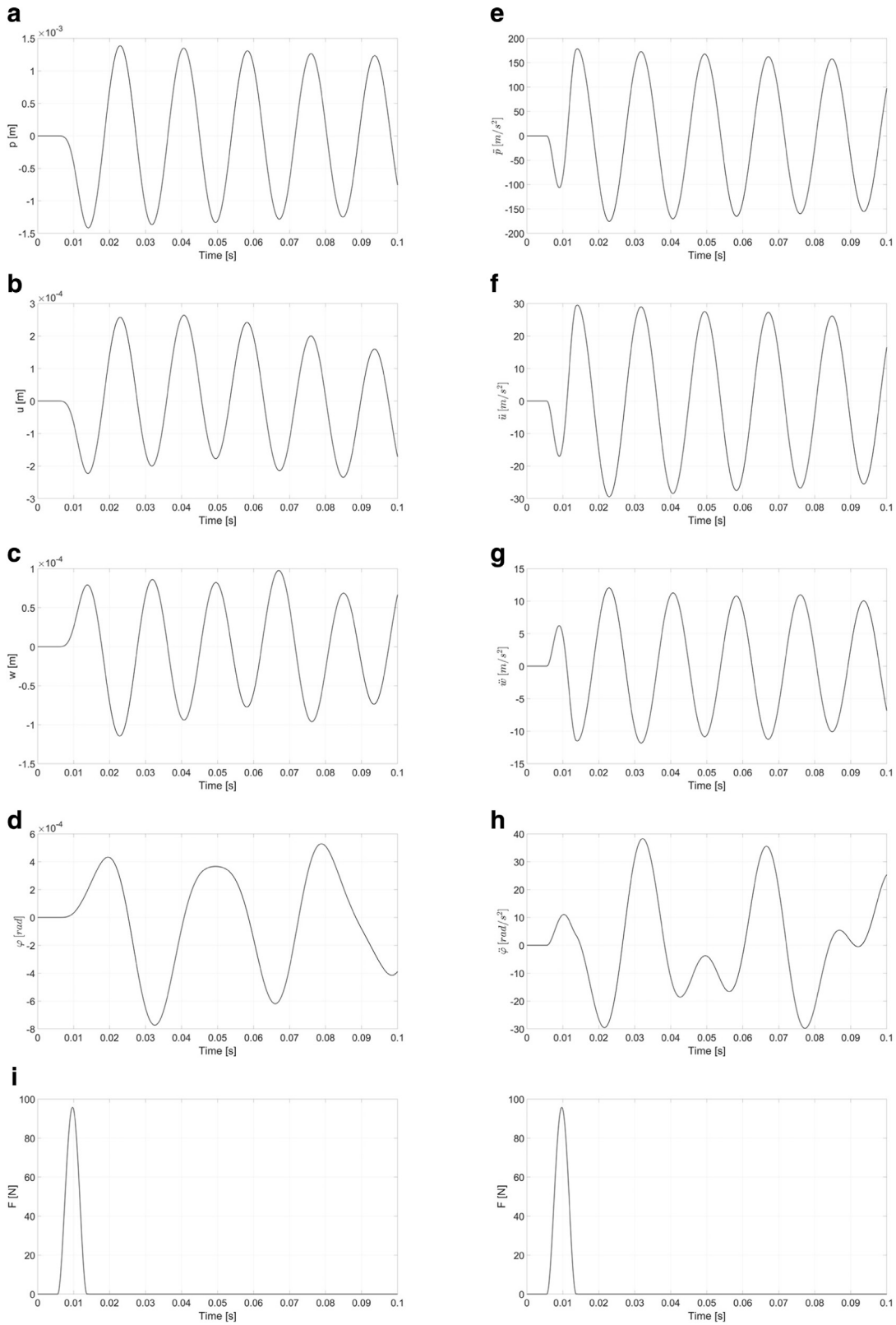

Fig. 10. Responses of the simulated conveyor within time interval $[0, 100]$ ms immediately after the excitation current pulse: (a)–displacement p, (b)–displacement u, (c)–displacement v, (d)–deflection (angle of rotation) φ, (e)–acceleration $\ddot{p}$, (f)–acceleration $\ddot{u}$, (g)–acceleration $\ddot{v}$, (h)–acceleration $\ddot{\varphi}$ and (i)–excitation force.

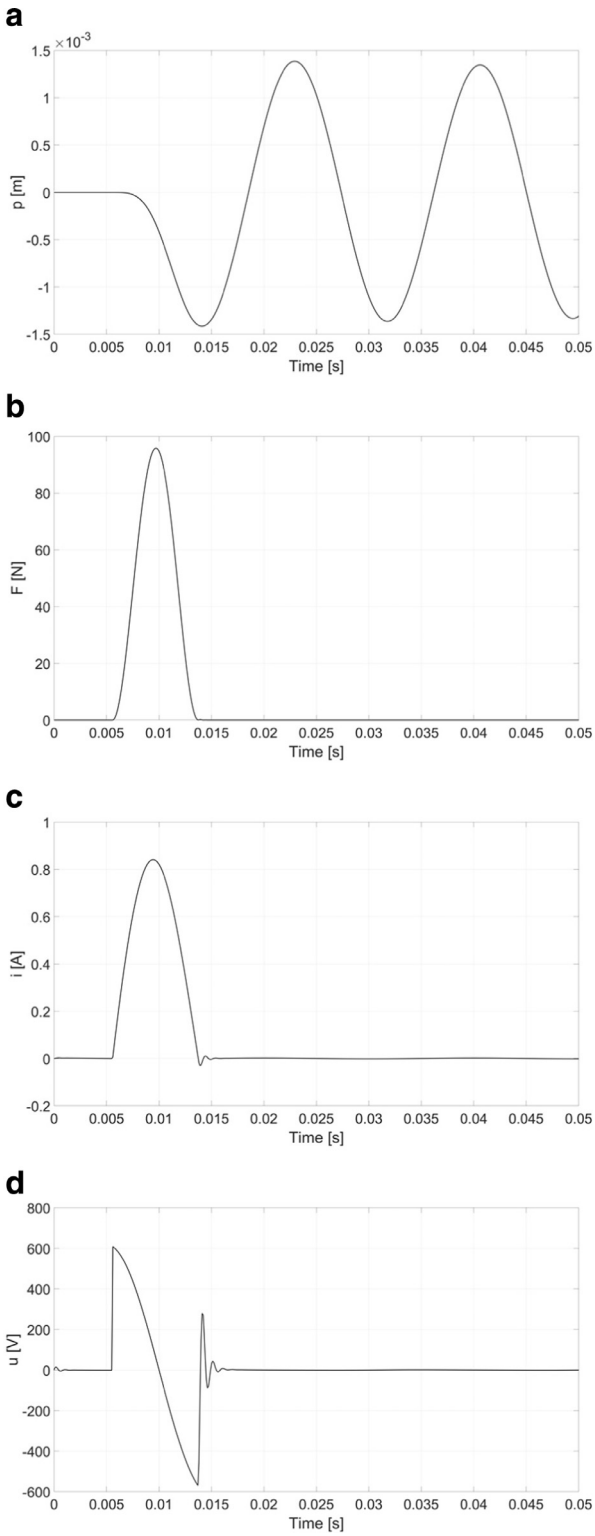

Fig. 11. Response of the simulated vibratory conveyor and EVA within time interval [0,50] ms immediately after the excitation current pulse: (a)–displacement p, (b)–EVA excitation force, (c)–EVA current and (d)–EVA voltage.

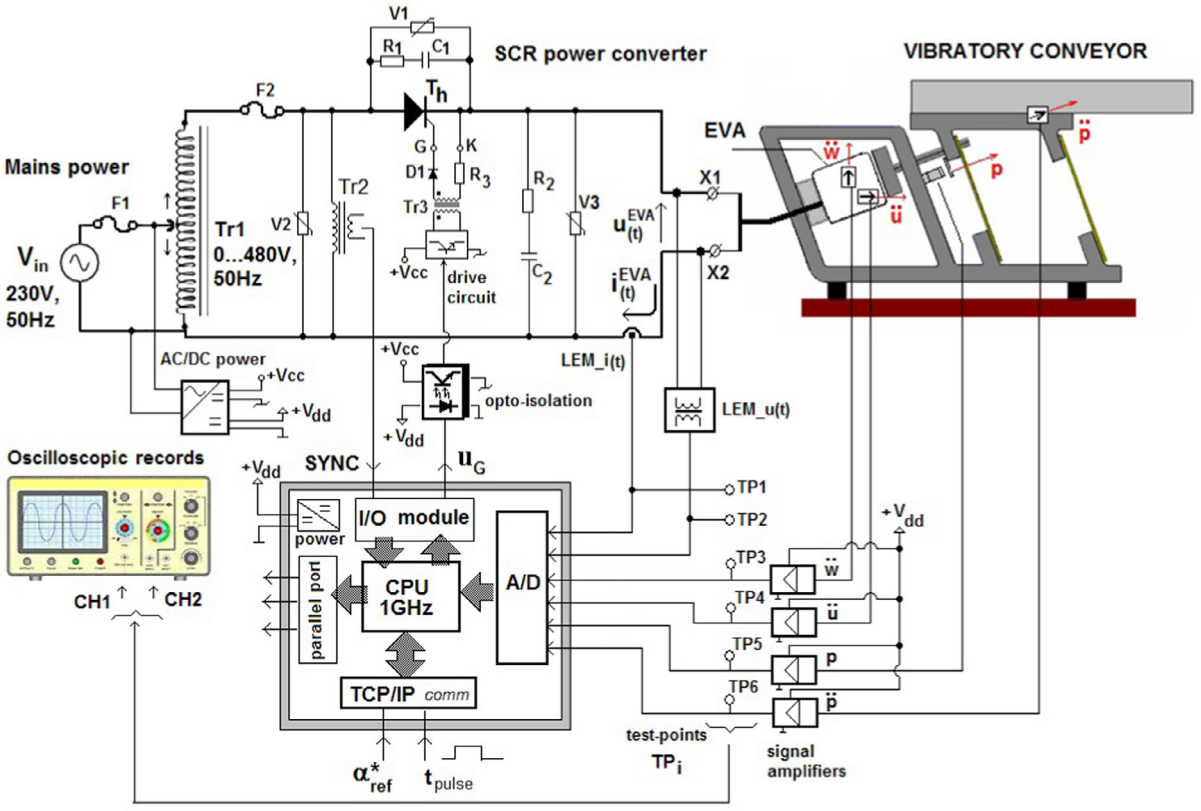

Fig. 12. Schematic block diagram of the experimental setup.

protective functions are realized: over-current protection of the thyristor by ultra-fast fuse *F*2, protection from excessive rate of voltage increase ("*dv*/*dt*") between anode and cathode of the thyristor by the resistive-capacitive snubber circuit R_1-C_1 and varistor *V*1, protection from the mains transient over-voltages by varistor *V*2, as well as protection circuit against transient over-voltages due to load (R_2-C_2 and varistor *V*3). The transformer *Tr*2 is used for synchronization of the control circuit with mains power. Thyristor pulse excitation is realized by short positive voltage pulses of the specific slope and amplitude, provided by pulse transformer *Tr*3. Galvanic isolation of the power source (440 V, 50 Hz) from the control circuit is also accomplished by this transformer. Diode *D*1 provides a positive voltage pulses in the gate circuit, while resistor *R*3 limits the gate current of the thyristor. Primary side of the pulse transformer is excited by transistor driver circuit which is galvanically isolated from the control circuit by a transistor opto-coupler circuit.

Measuring part of the system is composed of two sensors intended for measuring electrical quantities: EVA voltage and EVA current and four sensors intended for measuring mechanical quantities: base accelerations in the *u* and *w* directions ($\ddot{u}$ and $\ddot{w}$), acceleration of the vibratory trough in the direction of relative displacement *p* ($\ddot{p}$), as well as displacement *p*.

Measurement of EVA current is realized by *LEM* current sensor $LA-25N$ based on closed loop current transducer using *Hall effect*, where the range of the measured current at the primary side is $[-5, 5]$ A, the conversion ratio is 1: 200, and bandwidth is DC to 150 KHz. Voltage isolation between the primary and secondary (measuring) sides is 2.5 kV. The sensor is supplied by ± 15 VDC. The output measuring resistor is designed to provide output voltage range of $[0, 10]$ VDC for the current range of $[-5, 5]$ A. Note that value of 5 VDC corresponds to zero current level. The output voltage signal obtained in this way is brought to A/D converter of the control device.

The EVA voltage measurement is realized by *LEM* voltage sensor *LV* 100–1000/*SP*9 based on closed loop voltage transducer using *Hall effect*, where the range of measured voltages at the primary side is $[-1500, 1500]$ V, turns conversion ratio is 10000:2000, and the bandwidth is DC to 10 KHz. Voltage isolation between the primary and measurement sides is 6 kV. The sensor is supplied by ± 15 VDC.

The output measuring resistor is designed to provide output voltage range of $[0, 10]$ VDC for the voltage range of $[-1500, 1500]$ V on the primary side. Note that value of 5 VDC corresponds to the zero voltage level on the primary side. The measured signal is brought to *A*/*D* converter of the control device.

The acceleration measurements are accomplished by acceleration sensors *HBM-B*12/200 over the acceleration range $[0, 20]$ g and frequency range of $[0, 200]$ Hz. Signals from the accelerometer are amplified to voltage level 0–10 VDC by an electronic transducer (electronic amplifier + filter), and then brought to *A*/*D* converter of the controller.

The measurement of displacement p is realized by contactless inductive sensor $Ni10-18-LiU-H1141$ (manufactured by *Turck*) for displacement range of $[1, 7]$ mm, together with an amplifier of analog output range $[0, 10]$ VDC, and bandwidth up to 100 Hz.

Displaying and recording of the characteristic measured signals at test points $TP1$–$TP6$ are achieved by a two-channel digital storage oscilloscope *PM*3350 *PHILIPS* /50 MHz /100 Ms /sec.

The control device is based on modular *PC* 104 system. The basic elements of this device are: power supply ±12 VDC/1A, 5 VDC/8 A, 1 GHz *CPU*, input output (*I/O*) module, analog input module with analog/digital (*A/D*) 12-bit conversion, parallel port and input module for *TCP/IP* communication, which is used for setting the values of parameters: α^*_{ref} – the controllable phase angle and t_{pulse} – width of the excitation pulse-train at the thyristor gate.

Control of the period and amplitude of the single sinusoidal current pulse for excitation of the EVA is accomplished by a control circuit. One sine current pulse of 1 A amplitude and short duration (4–8 ms) is sufficient to induce oscillation of the vibratory conveyor, which further allows detecting the base acceleration in the u and w directions ($\ddot{u}$ and $\ddot{w}$), acceleration of the vibratory trough in the direction of the relative displacement p ($\ddot{p}$), as well as relative displacement p. In fact, this current pulse produces a square-sine pulse excitation force $\vec{F}$ obtained by attracting and releasing the EVA armature (anchor). In this way, it is possible to obtain the maximum value of the excitation force of approximately 90 N and duration of about 8 ms. The time moment of thyristor triggering is determined by the phase angle α^*, which is calculated from the time moment of the supply voltage zero crossing (i.e. *zero crossing detection*). The zero crossing detection is achieved by means of the synchronization transformer $Tr2$ and electronic circuit within the I/O module of the control system. The assigned value of phase angle α^* must be inside interval $10^\circ - 160^\circ$. In order to ensure reliable turn-on of the thyristor, duration of the series of firing (excitation) pulses is set to 8 ms.

5.4. Experimental results

Fig. 13 presents the oscilloscopic records of the vibratory conveyor characteristic quantities upon excitation by a short EVA current pulse obtained by the described unidirectional power converter. The value of the phase angle α^* is set to 100°. Under these conditions, given electrical parameters of EVA, a current pulse of 8 ms duration and amplitude of 0.95 A is generated. Due to quadratic function between force $\vec{F}$ and EVA current, the applied current pulse induces a pulse of force of amplitude around 90 N and duration of 8 ms.

Fig. 13 (a) shows the oscilloscopic records of the displacement response of the vibratory trough. The amplitude of the response immediately after application of the excitation pulse is equal to 1.5 mm. Also, the oscilloscopic record shows that time constant of the displacement p is $\tau_p = 0.9$ s. Fig. 13(b) shows the oscilloscopic record of the vibratory trough acceleration $\ddot{p}$. It can be seen that the initial amplitude of the acceleration is equal to 18 g ($\approx 180\,\mathrm{m/s^2}$)). Time constant is the same as in the case of displacement p. Relationship between displacement amplitude p and acceleration $\ddot{p}$ is equal to the square of the dominant resonant angular frequency of the conveyor ($\omega_{res} = \sqrt{(\ddot{p})_{max}/(p)_{max}} = \sqrt{180/1.5 \cdot 10^{-3}}$ rad/s, i.e. linear resonant frequency is $f_r \approx 55$ Hz). Fig. 13(c) shows the oscilloscopic record of the vertical component of the base acceleration $\ddot{w}$. It can be observed that the initial value of this acceleration is approximately equal to 2 g ($\approx 20\,\mathrm{m/s^2}$). Oscilloscopic record of the horizontal acceleration components of the vibratory conveyor base is shown in Fig. 13(d). It can be noticed from the record that the initial value of the acceleration is approximately equal to 5 g ($\approx 50\,\mathrm{m/s^2}$). Time constants of both accelerations are equal to 0.9 s, as in the case of displacement p and acceleration $\ddot{p}$.

Fig. 14 presents the oscilloscopic records of the vibratory conveyor response immediately after the excitation current pulse, i.e. the excitation force pulse at the time interval of 100 ms. Fig. 14 allows reading the characteristic values of the vibratory conveyor response more accurately. The response of displacement p is given in Fig. 14(a). Amplitude of the displacement at the initial time instant is 1.5 mm. The period of displacement waveform is 18.7 ms, providing a more accurate value of the resonant frequency of 53.5 Hz. Oscilloscopic record of the vibratory trough acceleration $\ddot{p}$ is given in Fig. 14(b). Amplitude of the acceleration at the initial time instant is 17 g ($170\,\mathrm{m/s^2}$, which corresponds to the previously obtained values of displacement amplitude p (≈ 1.5 mm) and resonant frequency of 53.5 Hz. Acceleration responses of the vibrating conveyor base in the vertical and horizontal directions $\ddot{u}$ and $\ddot{w}$, respectively, are given in Fig. 14(c). Acceleration amplitudes $\ddot{u}$ of 4.8 g ($\approx 48\,\mathrm{m/s^2}$) and acceleration $\ddot{w}$ of 2 g ($\approx 20\,\mathrm{m/s^2}$) are clearly observed from Fig. 14(c). Oscilloscopic records of EVA voltage and current are presented in Fig. 14(d). It can be noticed that the phase angle is set to $\alpha = 100^\circ$ (time delay from the mains voltage zero crossing is 5.6 ms). Under these conditions, an approximately sinusoidal half-wave EVA current of 8 ms duration and 0.95 A amplitude, i.e. impulse excitation force F of 90 N and 8 ms time duration, is achieved. Since the observed time interval of all of the obtained typical responses in this experiment is 2 s, it may be concluded that the impulse excitation force approximately corresponds to Dirac excitation of the vibratory conveyor.

6. The conclusions

A mathematical model of the resonant linear vibratory conveyor with electromagnetic excitation is presented. Lagrange equations of the second kind are applied to derive dynamic model of the mechanical part of the vibratory conveyor. The system states are chosen to be: displacement of the vibratory trough, displacements of the base of the vibratory conveyor in the vertical and horizontal directions, and rotation of the base. Also, a mathematical model of the EVA is derived and

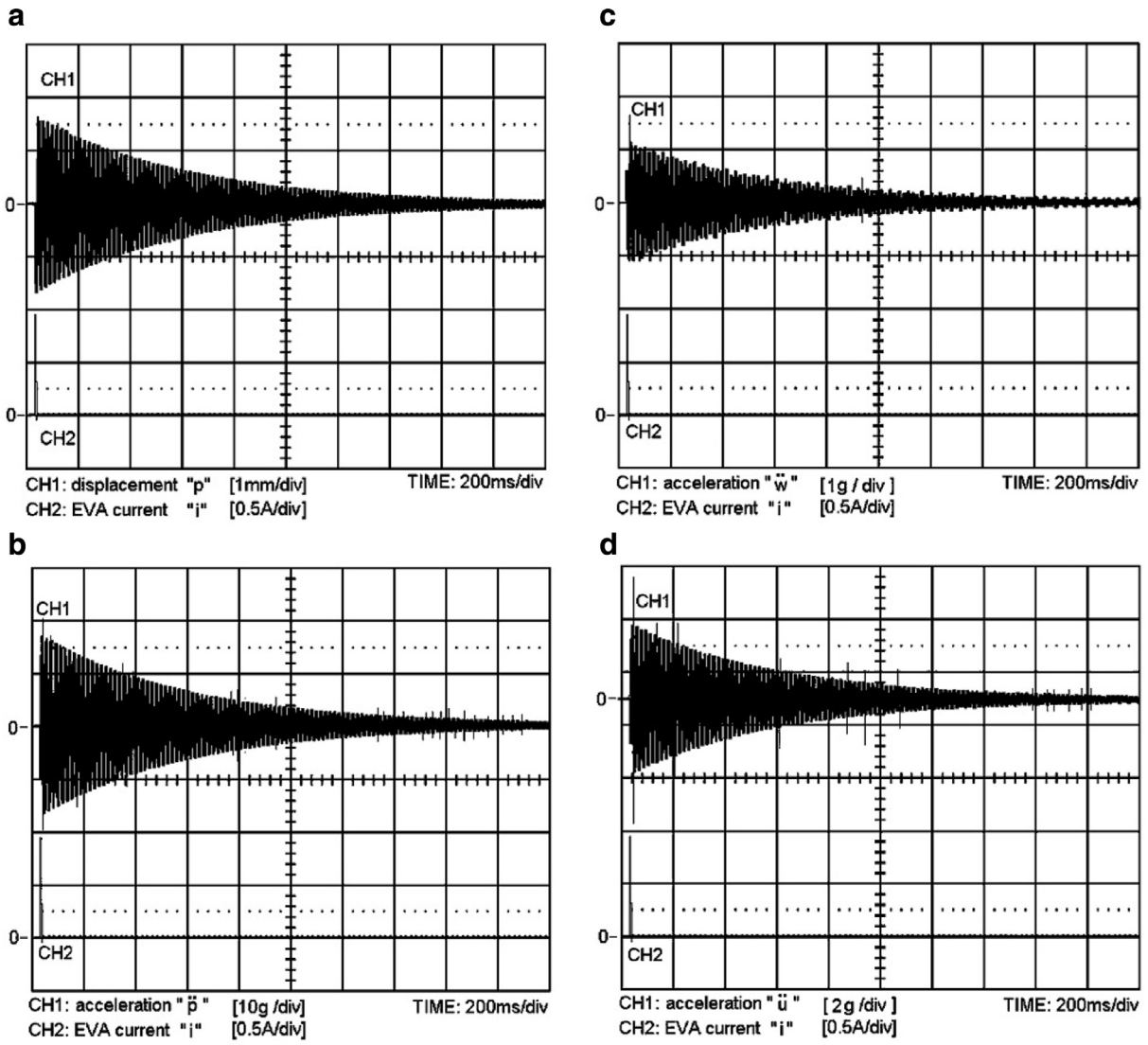

Fig. 13. Responses of the real vibratory conveyor to the impulse excitation: (a)–displacement p, (b)–acceleration $\ddot{p}$, (c)–acceleration $\ddot{w}$ and (d)–acceleration $\ddot{u}$.

used for obtaining the corresponding driving force. An electromagnetic vibratory actuator represents an electromechanical subsystem of the vibratory conveyor and its model has also been obtained based on application of Lagrange equations of the second kind.

The simulation of the vibratory conveyor has been carried out in order to examine system's behavior. The quantity and type of the transporting material have not been taken into consideration due to complexity of such analysis. Therefore, the simulations assuming an empty vibratory conveyor have been carried out throughout the paper. The displacements of the system and the corresponding accelerations have been obtained as a response to excitation by a pulse of force. Duration of the excitation force impulse is chosen to be quite short therefore it can be said that the applied pulse approximates Dirac excitation impulse.

A real experimental setup was built in order to verify the simulation results. Moreover, the experimental setup, including description of technical details, used sensors, and techniques for data measuring and acquisition are also presented in this paper. The measured signals include the displacements and the corresponding accelerations, previously obtained by the simulations. A comparison of the experimental and simulation results has been carried out. The experimental results are in a very good correlation with the simulations. Hence, it may be concluded that the mathematical model presented in this paper corresponds to the behavior of a real system.

The directions for further research will be to include the study of the robustness of the mechanical system and its sensitivity, which refers to the variation of mechanical parameters of the linear vibratory conveyor. In addition, further

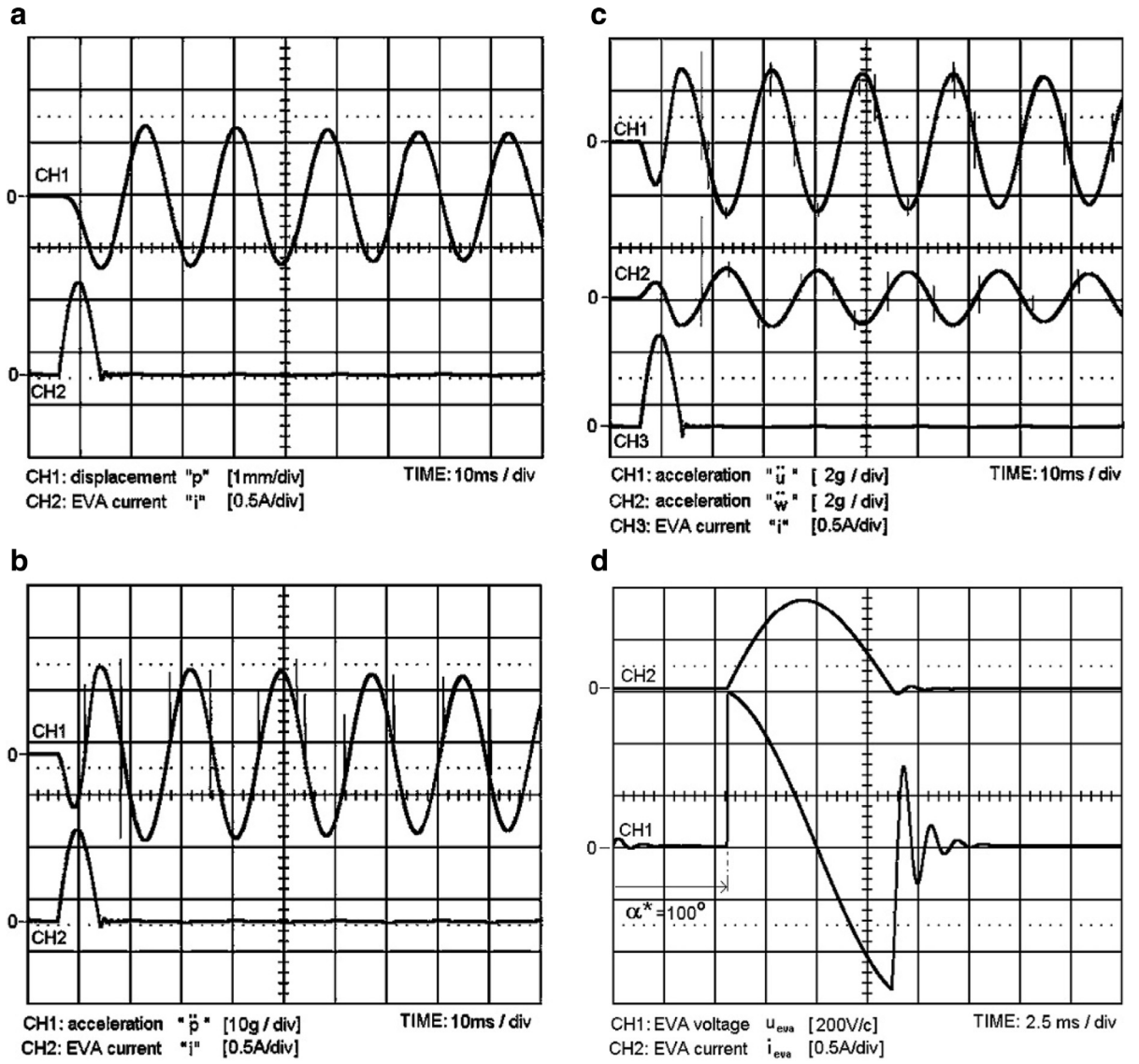

Fig. 14. The responses of the conveyor immediately after the excitation current pulse: (a)–displacement p, (b)–acceleration $\ddot{p}$, (c)–accelerations $\ddot{u}$ and $\ddot{w}$ and (d)–EVA voltage and current.

research will include investigation of the impact on the physical characteristics of conveying material (specific density, size particles and their granulation) on the process of vibratory transport, from a macroscopic point of view. The final goal is to increase the energy efficiency of vibratory conveying of bulk and particulate materials.

Acknowledgment

This investigation has been carried out with the financial support of the Serbian Ministry of Education, Science and Technological Development, within technological development projects: TR33022 and TR35046.

References

[1] I.F. Goncharevich, K.V. Frolov, E.I. Rivin, Theory of vibratory technology, Hemisphere Publishing Corporation, New York, 1990.
[2] M.E. Fayed, T.S. Skocir, Mechanical Conveyors: Selection and Operation, Technomic Publishing Company, Inc, Lancaster, PA (USA), 1997. pp. 225–270
[3] D. McGlinchey, Vibratory conveying under extreme conditions: An experimental study, in: Advanced in Dry Processing 2002, Powder/Bulk Solids, 2001, pp. 63–67.
[4] H. Kawamoto, A. Shigeta, M. Adachi, Utilizing electrostatic force and mechanical vibration to obtain regolith sample from the moon and mars, J. Aerosp. Eng. 29 (1) (2016).
[5] T. Dyr, P. Wodzinski, Model particle velocity on a vibrating surface, Physicochem. Probl. Miner. Process. 36 (2002) 147–157.

[6] E.M. Sloot, N.P. Kruyt, Theoretical and experimental study of the conveyance of granular materials by inclined vibratory conveyors, Powder Technol. 87 (3) (1996) 203–210.
[7] G. Soto-Yarritu, A. Martinez, Computer simulation of granular material: vibrating feeders, Powder Handl. Process. 13 (2) (2001).
[8] Z. Despotovic, Z. Stojiljkovic, Power converter control circuits for two-mass vibratory conveying system with electromagnetic drive: simulations and experimental results, IEEE Trans. Ind. Electron. 54 (1) (2007) 453–466.
[9] T. Doi, K. Yoshida, Y. Tamai, K. Kono, K. Naito, T. Ono, Modelling and feedback control for vibratory feeder of electromagnetic type, J. Robot. Mechatron. 11 (5) (1999) 563–572.
[10] T. Doi, K. Yoshida, Y. Tamai, K. Kono, K. Naito, T. Ono, Feedback control for vibratory feeder of electromagnetic type, in: Proceeding in ICAM'98, 1998, pp. 849–854.
[11] Z.V. Despotovic, A.I. Ribic, V. Sinik, Power current control of a resonant vibratory conveyor having electromagnetic drive, J. Power Electron. 12 (4) (2012a).
[12] Z. Despotovic, A. Ribic, M. Terzic, A comparison of energy efficiency of SCR phase control and switch mode regulated vibratory conveying drives, in: Proceeding 9th International Symposium Industrial Electronics -INDEL 2012, Banja Luka, Bosnia and Herzegovina, 1–3.XI, 2012b. http://www.indel.etfbl.net/2014/resources/Proceedings_2012/xPaper_17.pdf
[13] I.J. Sokolov, V.I. Babitsky, N.A. Halliwell, Autoresonant vibro-impact system with electromagnetic excitation, J. Sound Vib. 308 (2007) 375–391.
[14] A.I. Ribic, Z. Despotovic, High-performance feedback control of electromagnetic vibratory feeder, IEEE Trans. Ind. Electron. 57 (9) (2010) 3087–3094.
[15] D.G. Luenberger, Observing the state of a linear system, IEEE Trans. Mil. Electron. 8 (1964) 74–80.
[16] D.G. Luenberger, An introduction to observers, IEEE Trans. Autom. Control 16 (6) (1971) 566–602.
[17] 2003, Complete Guide to Vibratory Feeders and Conveyors, How To Choose and Use Vibratory Feeders and Conveyors, ERIEZ Magnetics, Pennsylvania, USA, pp. 3–13.
[18] Shames, H. Irving, A.F. Cozzarelli, Elastic and Inelastic Stress Analysis, Revised Printing, Taylor and Francis, Philadelphia, PA, 1997.
[19] Spring manual for Vibratory Conveyors and Feeder, The use of Composite Leaf Springs in Vibrating Machinery, HEATHCOTE INDUSTRIAL PLASTICS, Vol. I, Newcastle-under-Lyme, 2004. http://www.heathcotes.com. 1–16
[20] User' Guide for Short Carbon Fiber Composites, ZOLTEC COMPANIES, INC, St. Louis. 2000,
[21] A.K. Olsson, Finite Element Procedures in Modelling the Dynamic Properties of Rubber, printed by KFS i lund AB, lund, sweden, 2007 doctoral thesis.
[22] T.I. Rivin, Passive Vibration Isolation, ASME Press, 2003.
[23] B.G. Korenev, L.M. Reznikov, Dynamic Vibration Absorbers: Theory and Technical Applications, John Wiley and Sons, 1993.
[24] K.Y. Sanliturk, H.T. Belek, Design and Implementation of a 2-Dimensional Vibration Absorber on Pre-Heater Tower at A Cement Factory.
[25] S. Seely, Electromechanical energy conversion, McGraw-HILL Book Company INC., New York, 1962.
[26] V. Gourishankar, D.H. Kelly, Electromehanical energy conversion, Billing and Sons Ltd., Guldford & London, London, 1973.
[27] L. Meirovitch, Fundametals of Vibrations, Mc.Graw Hill International Edition, Mechanical Engineering, New York, 2001.
[28] H.E. Koening, W.A. Blackwell, Electromehanical system theory, McGRAW-HILL Book Company INC., New York, 1961.
[29] S.B. Dewan, A. Straughen, Power Semiconductor Circuits, John Willey & Sons, 1975.
[30] M.H. Rashid, Power Electronics Handbook, Third edition, Butterworth-Heinemann, 2011.
[31] Matlab, 2016, Informations available online on: URL http://www.mathworks.com/products/matlab/, MATLAB documentation,